

Electronic Thesis and Dissertation Repository

12-14-2021 2:00 PM

Lunar Regolith Simulant Behaviours Affected by Shock Metamorphism and Mineralogy

Xiao Chen Zhang, *The University of Western Ontario*

Supervisor: Osinski, Gordon R., *The University of Western Ontario*

A thesis submitted in partial fulfillment of the requirements for the Master of Science degree in Geology

© Xiao Chen Zhang 2021

Follow this and additional works at: <https://ir.lib.uwo.ca/etd>



Part of the [Geology Commons](#), and the [Geotechnical Engineering Commons](#)

Recommended Citation

Zhang, Xiao Chen, "Lunar Regolith Simulant Behaviours Affected by Shock Metamorphism and Mineralogy" (2021). *Electronic Thesis and Dissertation Repository*. 8329.
<https://ir.lib.uwo.ca/etd/8329>

This Dissertation/Thesis is brought to you for free and open access by Scholarship@Western. It has been accepted for inclusion in Electronic Thesis and Dissertation Repository by an authorized administrator of Scholarship@Western. For more information, please contact wlsadmin@uwo.ca.

Abstract

There are still many gaps in improving the fidelity of lunar regolith simulants to simulate more properties. This study compares some fundamental physical and mineralogical properties of three types of lunar highland regolith simulants: LHS-1, a commercial product with high mineralogical fidelity; UWO-1G, an original simulant that is the main component of LHS-1; and UWO-1S, another original product that is attempted to produce shocked grains in lunar simulants from pulverizing and mixing impact rocks sourced from the Mistastin Crater.

Preliminary results indicated that even though all simulants are composed of mostly plagioclase minerals and have similar particle size distribution patterns, the UWO-1S grains exhibit less angularity compared to LHS-1 and UWO-1G, as well as poor ability to regain void ratio during consolidation tests. Both are indications that the grain strength is possibly weaker due to impact events, however further characterizations are also recommended for more evidence.

Keywords

Lunar geology, lunar simulants, ISRU, impact cratering, shock metamorphism

Summary for Lay Audience

The interest in returning to the Moon, and potentially building habitats and other infrastructures, has been rising globally. Past lunar exploration, such as USA's Apollo crewed landing missions and autonomous sample return missions from the former USSR's Luna Program, and China's Chang'e Program, have determined that lunar regolith could be a critical hazard but also a valuable resource. In order to design future equipment for safe and sustainable lunar exploration, dozens of simulated lunar regolith, or "simulants", have been produced worldwide for testing materials that will come into contact with lunar regolith.

However, lunar regolith is a complex product resulting from being exposed to the harsh space environment. Repetitive impact events and space radiation resulted in many unique features within lunar regolith that are difficult or even impossible to simulate. Therefore, current simulants mostly only replicate one or a few properties of lunar regolith for specific research purposes.

In this research, three types of lunar highland simulants were selected to compare some of their fundamental properties, which focuses on the discussion of the role of mineralogical accuracy and shocked grains within lunar simulants. We chose LHS-1, which is a commercial product that aims at high mineralogical fidelity, created UWO-1G, which only used one type of feedstock that is the main component of LHS-1, and created UWO-1S, which attempted to produce shocked grains from pulverizing impact rocks.

Preliminary comparison results confirmed that these simulants contain very similar mineralogical components, and their particle size distributions are closely matched to allow a fair comparison of physical properties. LHS-1 and UWO-1G did not differ from each other too much, but UWO-1S demonstrated weaker physical strengths, which could imply that the grain durability is weaker than the other two. Further characterizations and additional comparative samples are suggested to strengthen the evidence.

Acknowledgments

There are too many people that have helped me through a rough time during this program. I would like to thank my supervisor, Dr. Gordon Osinski, for giving me this opportunity that I once thought was impossible. I also want to thank Oz for the understanding, encouragement and support that meant a lot to me when finishing this degree.

I would also like to thank Dr. Timothy Newson for allowing me using the facilities at the Department of Civil Engineering and openness for collaboration. I also cannot be grateful enough for my wonderful simulant buddy Devansh Joshi on all the help and explanation during geotechnical characterizations and providing me with results while I stepped away for a special summer program.

Many thanks to Stephen Wood for teaching me how to use the rock crusher and pulverizer so I could attempt creating the samples by myself for this study, as well as for helping with making the thin sections. Thanks to Dr. Vahid Dehnavi at Surface Science Western for his help with running XRD characterization, and appreciation for my friend Fengke Cao and his supervisor, Dr. Roberta Flemming, for the instruction on processing mineralogical identification for this study. Also many thanks to Dr. Todd Simpson at the Western Nanofabrication Facility for helping with SEM imaging.

I finished this master's degree while attending the Space Studies Program 2021 back at the International Space University, my alma mater, as a Teaching Associate. It was a very special time where I met and worked with a group of exceptional participants and staff members. To my co-chairs and participants of the Team Project *Solutions for Construction of a Lunar Base*, you all lifted me up from a difficult time and made me a different person in just two months. Although we experienced a very tragic event together during this program, we embraced each other during this very tough time, which brought us even closer. I will forever cherish this summer and sincerely wish a successful future for everyone.

Finally, I want to thank my family and friends for their continuous support that encouraged me to pursue a field that I truly love.

Table of Contents

Abstract.....	ii
Summary for Lay Audience.....	iii
Acknowledgments.....	iv
Table of Contents.....	v
List of Tables.....	vii
List of Figures.....	viii
List of Appendices.....	xii
Chapter 1.....	1
1 Introduction.....	1
1.1 Overview of the Moon.....	3
1.2 Lunar Regolith and its Characteristics.....	5
1.2.1 Evolution and composition of the lunar surface.....	7
1.2.2 Lunar Regolith Evolution and Components.....	9
1.2.3 Physical and Geotechnical Properties.....	15
1.3 Lunar Regolith Hazards and potential ISRU uses.....	18
1.4 Lunar Regolith Simulants and Their Limitations.....	20
1.5 Statement of Motivation.....	22
Chapter 2.....	24
2 Methods.....	24
2.1 Sample description.....	25
2.1.1 LHS-1 by Exolith Lab.....	25
2.1.2 Original simulant UWO-1S.....	27
2.1.3 Original simulant UWO-1G.....	37
2.2 Particle Shape.....	41

2.3 Particle Size Distribution	42
2.4 Mineralogy Identification	46
2.5 Specific Gravity	49
2.6 Density, Void Ratio	51
2.7 Consolidation	53
Chapter 3.....	57
3 Results	57
3.1 Mineralogy	57
3.2 Particle Shape.....	59
3.3 Particle size distribution.....	61
3.4 Density, void ratio, and specific gravity	63
3.5 Consolidation	64
Chapter 4.....	66
4 Discussions.....	66
4.1 Mineralogy	66
4.2 Physical properties	66
4.3 Other considerations	68
4.4 Potential future work.....	68
Chapter 5.....	70
5 Conclusions	70
References.....	73
Appendices.....	86
Curriculum Vitae	94

List of Tables

Table 1. Overview of potential lunar resources (Guo et al., 2013).....	2
Table 2. Physical data comparison of the Moon and Earth (Vaniman et al., 1991).	3
Table 3. Chronological order of physical lunar samples brought back by space missions. Apollo and Luna mission details were edited from van Kan (2011). Sources for Chang’e-5 are Qian et al., (2021) and Xu, Guo and Liu (2021).....	5
Table 4. Lunar regolith average porosity, void ratio and bulk density at various depths (NASA, 2019; Carrier, Olhoeft and Mendell, 1991).	17
Table 5. Examples of some lunar regolith simulants and their intended purpose(s).	21
Table 6. General information of samples used in this study.....	24
Table 7. Mineralogical composition as mixed of LHS-1 as indicated on its product datasheet (Exolith Lab, 2021).	27
Table 8. Examples of milling steps applied to produce lunar simulants in large quantities.	34
Table 9. Number and sizes of the sieves used to characterize PSD for this study.....	42
Table 10. Plagioclase mineral group (Haldar, 2020).	46
Table 11. Maximum and minimum densities and void ratios, and specific gravity of each simulant. Information of lunar regolith was taken from Carrier, Olhoeft and Mendell, (1991), OPRH2N taken from Zhang, et al. (2019) and Newson et al. (2021).....	64

List of Figures

Figure 1. Apollo 11 astronaut Edwin “Buzz” Aldrin standing beside a leg of the Landing Module during an extra-vehicular task, leaving footprints on the loose regolith. NASA photo AS11-40-5902 (NASA History Office, 2007).....	3
Figure 2. Sites of lunar sample return missions. The numbers 11-17 (without 13) indicate Apollo landing missions. Edited based on Wright (2019).....	6
Figure 3. Illustration of the Lunar Magma Ocean and the current understanding of lunar mantle and crust compositions (Geiss and Rossi, 2013).....	7
Figure 4. Basaltic magma in the olivine-pyroxene mantle extrudes onto the lunar surface through fractured channels to form lunar mare (O’Hara, 2018).	8
Figure 5. Lunar albedo mapped by the Lunar Orbiter Laser Altimeter (LOLA) on board the Lunar Reconnaissance Orbiter (LRO) at 1064nm wavelength. Top left: near side; top right: far side; bottom left: north pole view; bottom right: south pole view (Lucey et al., 2014).	9
Figure 6. Space weathering processes that shaped regolith grains on the lunar surface (Noble, 2009).	11
Figure 7. A portion of the rock fragments from Apollo 11 regolith sample, dominated by basaltic components as the mission was carried out at a lunar mare (Korotev, 2021).	12
Figure 8. Close-up look of agglutinate particles that shows the irregular, porous, and ropey shape (a-e), as well as the np-Fe mounds on the surface of one agglutinate particle (f) (McKay et al., 1991).	13
Figure 9. Lithic fragment composition of selected lunar regolith samples, except 24999 was from Luna 24 (Simon and Papike, 1981).....	14
Figure 10. Sorting, grain size and agglutinate content relationship within 42 Apollo 17 regolith samples (McKay et al., 1991).....	15

Figure 11. SEM images of Apollo 17 Sample 70051 dust particles, showing complex features such as the porous (“Swiss-cheese”) and “ropey” structures (Liu et al., 2006)..	16
Figure 12. Particle size distribution among different Apollo and Luna landing missions (Mitchell et al., 1972).....	17
Figure 13. He-3 abundance on the near side and far side within the top 1 μm of lunar regolith, constructed with Clementine UV/VIS multispectral data (Fa and Jin, 2007)....	19
Figure 14. LHS-1 lunar highland simulant from the Exolith Lab.....	26
Figure 15. Satellite image of the Mistastin Crater from the Landsat 8 Operational Land Imager, taken in September 2017 (NASA Earth Observatory, 2017).	28
Figure 16. Geologic map of the Mistastin Crater. Red boxes indicate the locations South Creek and Discovery Hill where the feedstocks were collected from. Bottom right: Location of the crater in Labrador, Canada. Modified from Pickersgill, Osinski and Flemming (2015), based on previous studies of Marion and Sylvester (2010), Grieve (1975) and Currie (1971).	29
Figure 17. Formation process of the Mistastin Crater (Hill, Osinski and Banerjee, 2020)	30
Figure 18. Examples of An-rich breccia from South Creek.	31
Figure 19. Thin section images of an anorthosite breccia used to create UWO-1S. PDFs (a, b) and melting grain boundaries (c, d) could be observed, confirming the description in Hill, Osinski and Banerjee (2020). In addition, irregular fractures can also be observed in all images.	32
Figure 20. Examples of the melt rocks from Discovery Hill, used to create UWO-1S....	33
Figure 21. Thin section images of an impact melt rock used to create UWO-1S. (a), (b) and (d) can be seen with fine-grained groundmass with small crystals or glassy components. Impact crystalline features are seen in (c).	33

Figure 22. Bico Chipmunk Crusher (Left) and T.M. Vibratory Ring Pulverizer (Right).	35
Figure 23. Rocks (impact melt rocks pictured) were tossed into the Bico crusher (upper left) and crushed into smaller masses (upper right), then transferred into the ring pulverizer container (lower left) to be ground into powder-like product (lower right). ...	36
Figure 24. Pulverized breccia (left) and melt rock (right).	37
Figure 25. Greenland anorthosite "Greenspar" provided by Hudson Resources Inc., before processing.	38
Figure 26. Geologic map of Greenland (White et al., 2016). Red arrow indicates the approximate location of the White Mountain Greenspar mining site.	40
Figure 27. Finished product of UWO-1G.	41
Figure 28. (Left) Assembled sieve stack; (Middle) Sample (UWO-1G pictured) added from the top (No. 4) sieve; (Right) Stack placed into a mechanical shaker to sift for 12 minutes.	43
Figure 29. LHS-1 Particle size distribution as provided on the product fact sheet (Exolith Lab, 2021).	44
Figure 30. Preparing for hydrometer test. 40g of sodium hexametaphosphate was weighed (upper left), and then added to 1L of distilled water (upper right). The container was then sealed and shaken to dissolve the solid (lower left) and the final solution was added to around 50g of the sifted fines (lower right, LHS-1 pictured).	45
Figure 31. Comparison of anorthite composition in terrestrial and lunar rocks (Papike, Taylor and Simon, 1991).	47
Figure 32. Bragg's law in XRD (Le Pevelen, 2010).	48
Figure 33. Sample grinding in preparation of XRD characterization. Sample shown in the figure is the Mistastin impact melt used to produce UWO-1S.	48

Figure 34. Example of different possible porosities within a lunar agglutinate (Carrier, Olhoeft and Mendell, 1991).....	49
Figure 35. (Left) De-airing 500ml distilled water in a volumetric flask; (Right) De-airing sample mixture (LHS-1 pictured) for 24h.	50
Figure 36. Sample (LHS-1 pictured) is loosely sprinkled into the mould through a funnel (left) and flattened with a spatula at the top (right).	52
Figure 37. Sample (LHS-1 pictured) was added to half the mould's depth (left) and vibrated for natural compaction with a weight to stop any loss in quantity (right). This step was repeated until the mould was fully filled with compacted sample.	53
Figure 38. Sample (LHS-1 pictured) was loosely sprinkled into the ring mould (upper left) and carefully flattened (upper right). After levelling, the mould was placed into a cylindrical container (lower left) and loaded into the oedometer for consolidation (lower right).....	55
Figure 39. XRD patterns with matched mineral candidates. The backgrounds are kept for demonstrating a slight curve within the breccia and UWO-1S around the range of 20 - 30°, which indicates the presence of glass.....	58
Figure 40. SEM images of LHS-1 (a,b), UWO-1G (c,d), UWO-1S breccia (e,f), UWO-1S melt (g,h), and UWO-1S mixed (i, j). Scale bars in the left column images are 20µm, and 10µm on the right column.....	60
Figure 41. Sieve analysis of simulant samples used for this study.	61
Figure 42. Hydrometer analysis of simulant samples used for this study.	62
Figure 43. Overall Particle size distribution of the simulant samples used for this study, combined with both sieve and hydrometer analysis results.....	63
Figure 44. Consolidation results of simulants.....	65

List of Appendices

Appendix A-1. Examples of large-scaled analogue sites (Foucher et al., 2021).....	86
Appendix A-2. Examples of small-scaled analogue samples (Foucher et al., 2021).....	87
Appendix A-3. Relevant functional analogues at each phase of a planetary exploration mission (Foucher et al., 2021).....	88
Appendix B. List of properties in lunar simulants in the order of importance in research. Ranking arranged based on consensus count of the 2005 Lunar Regolith Simulant Materials Workshop (Sibille et al., 2006).....	89
Appendix C. List of capability levels in replicating lunar regolith properties into simulants (LEAG and CAPTEM, 2010).....	91
Appendix D. Possible Sources of Errors and Contaminations	92
Appendix E: Consolidation Results	93

Chapter 1

1 Introduction

In the early 1960s, then-president of the United States John F. Kennedy, stated in a speech that, the US chooses to “go to the Moon by the end of the decade and do other things, not because they are easy, but because they are hard”. The ensuing Apollo Program demonstrated humanity’s capability to send astronauts on the Moon and return safely, which left a huge legacy that enabled the growth of science, engineering, physiology and many more disciplines related to the space sector. Decades later, with more countries participating in lunar exploration and NASA’s announcement of the Artemis Program, humanity’s interest of returning to the Moon is on the rise again, and many have been investigating the supporting technologies that would allow us to stay for a prolonged period.

To achieve this ambitious goal, it is widely believed that using local resources on the Moon to produce water and oxygen, build infrastructure and other critical components would be the most sustainable solution. This concept is commonly termed as in-situ resource utilization (ISRU), or space resource utilization (SRU). Success in this step could significantly reduce the cost of launching supplies from Earth and will accelerate humanity’s interplanetary settlement plans. ISRU is not only limited to the Moon but also considered for Mars, and possibly expanded to other celestial bodies in the future as well.

The surface of the Moon is covered with a loose, space-weathered material commonly referred to as the lunar regolith (e.g., see Figure 1), and is believed to be the reservoir of several types of resources such as metals, oxygen and helium-3. In the polar regions, observational data also suggests that local regolith might be mixed with large quantities of water ice. Guo, et al. (2013) summarized a list of lunar resources that can be utilized through processing lunar regolith, and other environmental advantages, as listed in Table 1.

This chapter provides a literature review on the evolution of the Moon and lunar regolith and introduces some fundamental parameters of lunar regolith from studying returned

samples. This discussion will lead to the introduction of the importance of studying regolith and lunar simulants, followed by an explanation of the project motivation.

Table 1. Overview of potential lunar resources (Guo et al., 2013).

	Resource	Potential Applications
Lunar Environment	Solar radiation	Power
	Near-vacuum atmospheric pressure	Material manufacturing
	Low gravity	Material manufacturing
Lunar Surface	Water ice	Propellant, life support
	Oxygen	Propellant, life support
	Hydrogen	Propellant, reactant
	Helium-3	Nuclear power
	Lunar regolith	Radiation shield
	Metals (e.g. iron, aluminum)	Construction, manufacturing
	Non-metals (e.g. silicon)	Solar panels, manufacturing
	Lava tubes	Heat and radiation shield

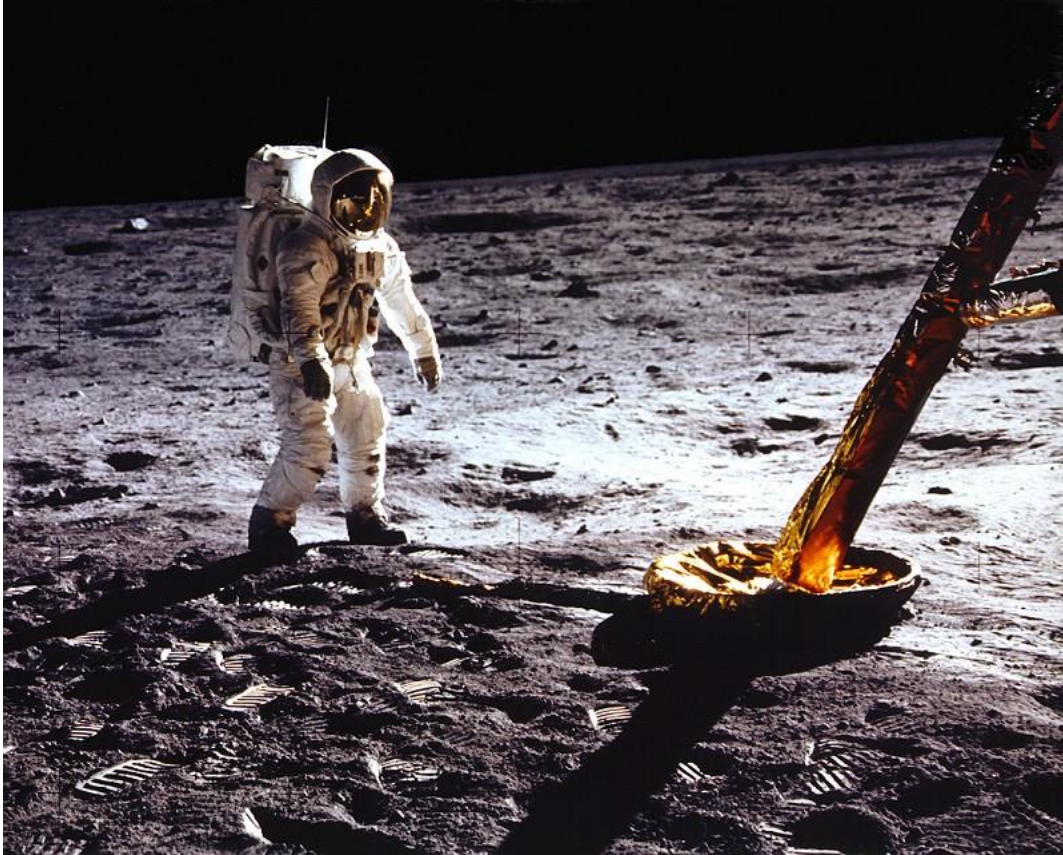


Figure 1. Apollo 11 astronaut Edwin “Buzz” Aldrin standing beside a leg of the Landing Module during an extra-vehicular task, leaving footprints on the loose regolith. NASA photo AS11-40-5902 (NASA History Office, 2007).

1.1 Overview of the Moon

The leading explanation of the Moon’s formation the Giant Impact Theory, which suggests that a Mars-sized body crashed into early Earth around 4.5 Ga, and the resulting debris remained in Earth’s orbit and eventually accreted to form the Moon (Hartmann and Davis, 1975; O’Hara, 2018; Hiesinger and Head, 2006). Despite the likelihood of originating from Earth, the Moon is drastically different from modern Earth. Some major differences are summarized in Table 2 by Vaniman, et al., (1991).

Table 2. Physical data comparison of the Moon and Earth (Vaniman et al., 1991).

Property	Moon	Earth
----------	------	-------

Mass (kg)	7.353×10^{22}	5.976×10^{24}
Spherical Radius (km)	1738	6371
Surface Area (km²)	37.9×10^6	510×10^6 , Land Area 149.8×10^6
Flattening¹	0.0005	0.0034
Mean Density (g/cm²)	3.34	5.517
Gravity at Equator (m/s²)	1.62	9.81
Escape Velocity at Equator (km/s)	2.38	11.2
Sidereal Rotation Time	27.322	23.9345
Inclination of Equator/Orbit	6°41'	23°28'
Mean Surface Temperature (°C)	107 (day), -153 (night)	22
Temperature Extremes (°C)	-233 to 123	-89 to 58
Atmosphere (Molecules/cm³)	$\sim 10^4$ (day), 2×10^5 (night)	2.5×10^{19}

¹ (Equatorial-ideal)/ideal radii

Moment of Inertia (1/MR²)	0.395	0.3315
Average Heat Flow (mW/m²)	~29	63
Seismic Energy (J/year)	2×10^{10} (or 10^{14}) ²	10^{17} to 10^{18}
Magnetic Field (A/m)	0 (small paleofield)	24 to 56

1.2 Lunar Regolith and its Characteristics

Lunar regolith has been studied for decades from remote sensing data and physical characterizations, either in-situ on the lunar surface or with samples brought back to Earth from the Apollo landing missions (USA), Luna 16, 20 and 24 (former USSR) and Chang’e-5 (China) (See Table 3 and Figure 2). This section introduces the major components of lunar regolith including mineralogical composition and commonly referenced physical parameters.

Table 3. Chronological order of physical lunar samples brought back by space missions. Apollo and Luna mission details were edited from van Kan (2011). Sources for Chang’e-5 are Qian et al., (2021) and Xu, Guo and Liu (2021).

Mission	Year	Landing Location	Approximate Sample Mass
Apollo 11	1969	Mare Tranquilitatis	21.6 kg
Apollo 12	1969	Oceanus Procellarum	34.3 kg

² Estimation for moonquakes only, does not include seismic events generated by meteoroid impacts.

Luna 16	1970	Mare Fecunditatis	101 g
Apollo 14	1971	Fra Mauro	42.3 kg
Apollo 15	1971	Hadley-Apennine	77.3 kg
Luna 20	1972	Apollonius highlands	50 g
Apollo 16	1972	Descartes	95.7 kg
Apollo 17	1972	Taurus-Littrow	110.5 kg
Luna 24	1976	Southern Mare Crisium	170 g
Chang'e-5	2020	Oceanus Procellarum	1731 g

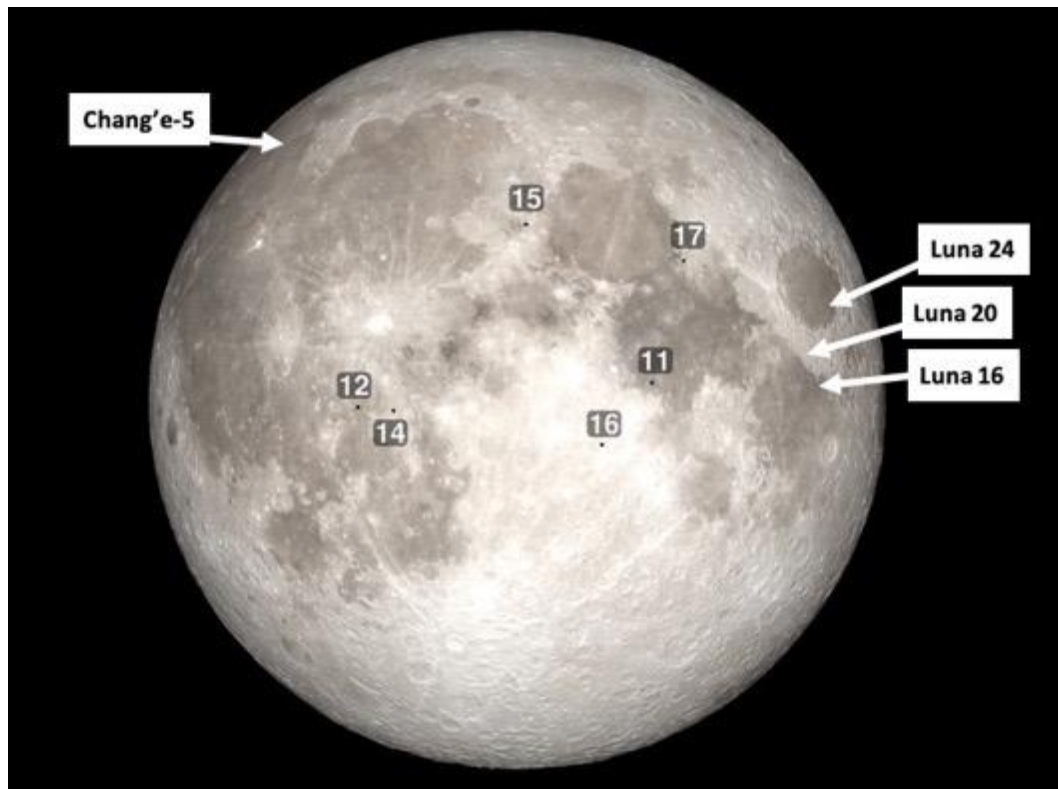


Figure 2. Sites of lunar sample return missions. The numbers 11-17 (without 13) indicate Apollo landing missions. Edited based on Wright (2019).

1.2.1 Evolution and composition of the lunar surface

The most widely accepted theory regarding the Moon's evolution after accretion is the Luna Magma Ocean Concept (Figure 3). The theory suggested that at the beginning of the Moon's formation, the entire body was in a magma state with all components molten and mixed due to the high temperature of the process. As the Moon cooled down over time, heavier components such as olivine and pyroxene started to crystallize first and sank to the bottom, forming the lunar mantle, leaving plagioclase components floating on top and eventually solidified to form the lunar crust (Wood et al., 1970; Cameron and Ward, 1976; Geiss and Rossi, 2013; Elardo, 2016; O'Hara, 2018; Elkins-Tanton, Burgess and Yin, 2011). Apart from olivine, pyroxene and plagioclase, a special group of incompatible elements called KREEP (potassium, rare earth elements, and phosphorous) were also believed to exist in between the crust and mantle, mostly within the basaltic layer (Geiss and Rossi, 2013; Ouyang, 2005; Warren, 1985).

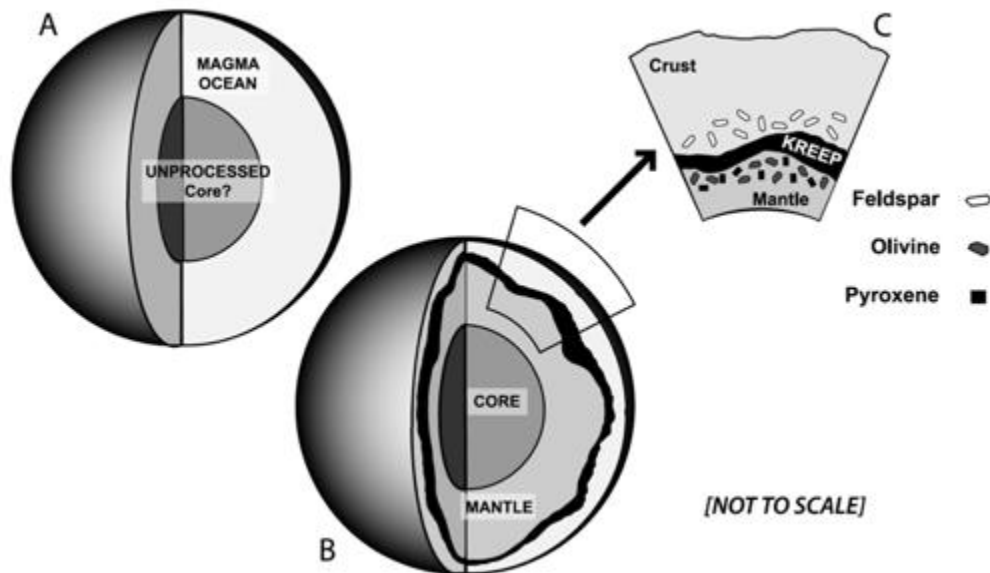


Figure 3. Illustration of the Lunar Magma Ocean and the current understanding of lunar mantle and crust compositions (Geiss and Rossi, 2013).

Lunar volcanism and early impact events such as the Late Heavy Bombardment Period (3.8-3.9 Ga) penetrated through, or fractured, the lunar crust and caused the mafic magma

flowing out to fill the impacted regions, which formed the dark-coloured lowlands as we see today (Figure 5). These plains are composed of mostly basaltic minerals of olivine and pyroxene and covers about 17% of the entire lunar surface (Head and Wilson, 1992; Gråe Jørgensen et al., 2009; O’Hara, 2018; Hörz et al., 1991). As ancient observers used to think of these features as seas or oceans on the Moon, these areas are now commonly referred to as lunar mare (plural form: maria), from the Latin language which means the sea. The original plagioclase crust, which are now seen as the light-coloured regions are commonly referred to as lunar highlands, or terra (plural form: terrae).

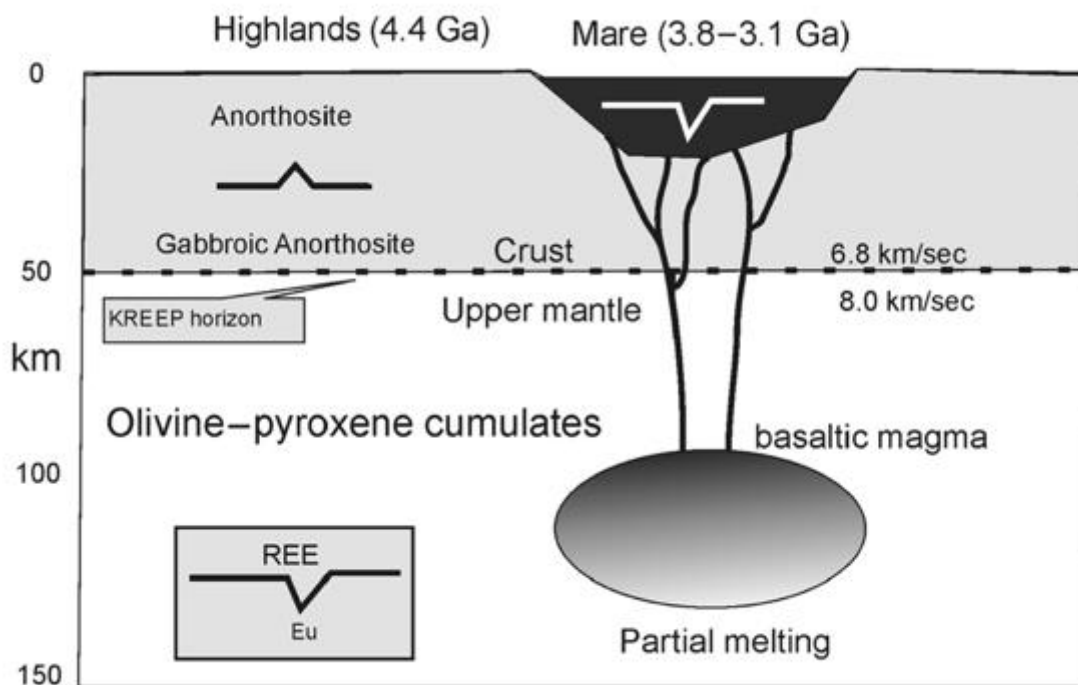


Figure 4. Basaltic magma in the olivine-pyroxene mantle extrudes onto the lunar surface through fractured channels to form lunar mare (O’Hara, 2018).

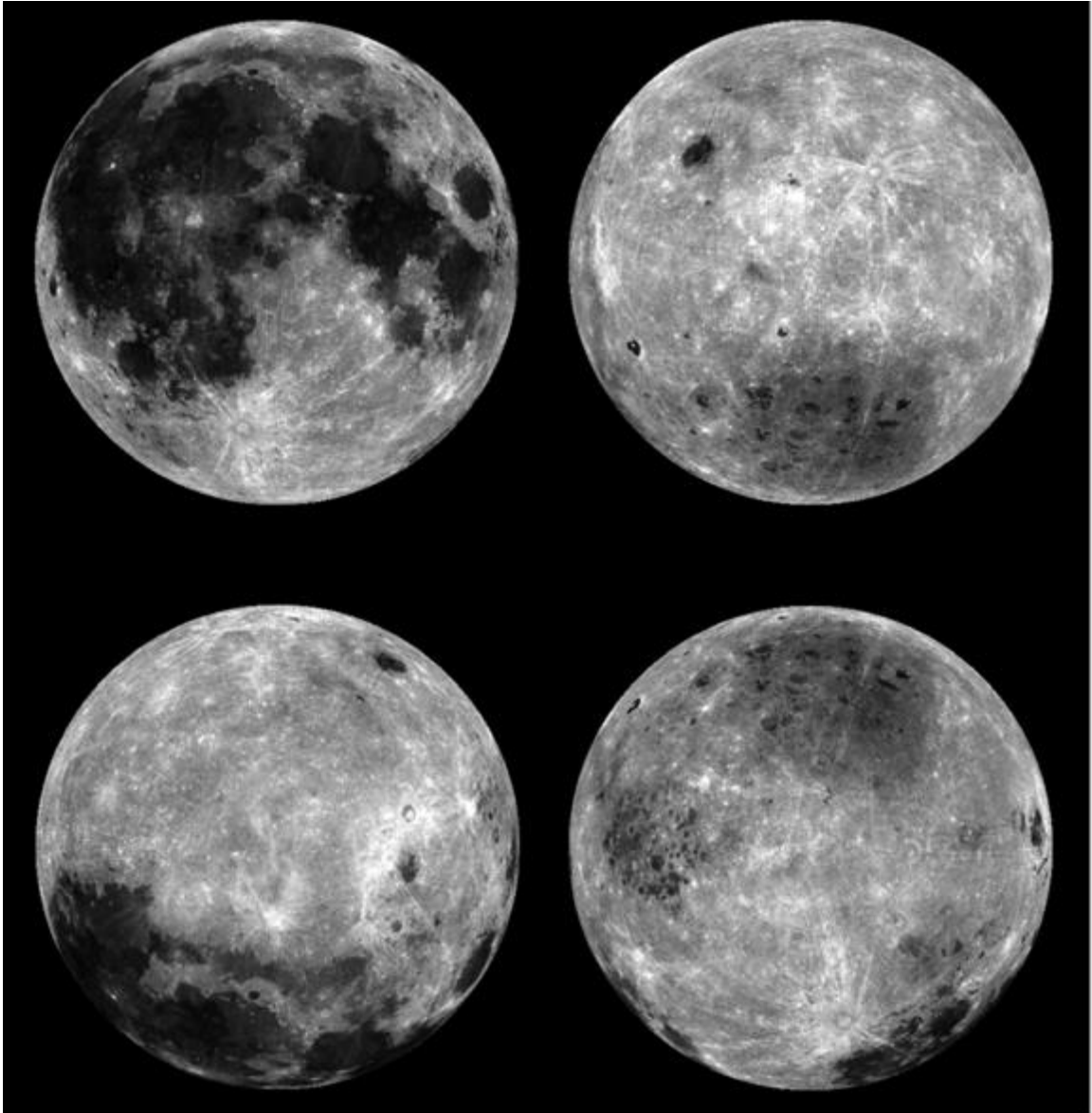


Figure 5. Lunar albedo mapped by the Lunar Orbiter Laser Altimeter (LOLA) on board the Lunar Reconnaissance Orbiter (LOR) at 1064nm wavelength. Top left: near side; top right: far side; bottom left: north pole view; bottom right: south pole view (Lucey et al., 2014).

1.2.2 Lunar Regolith Evolution and Components

Lunar regolith is the only layer that separates the lunar bedrock and deep space. Studying regolith is currently the only way to understand the lunar evolution and space environment (McKay et al., 1991).

Neuendorf, Mehl and Jackson (2005) defined lunar regolith as “a thin, grey layer on the surface of the Moon, perhaps several meters deep, consisting of partly cemented or loosely compacted fragmental material ranging in size from microscopic particles to blocks more than a meter in diameter. It is believed to be formed by repeated meteoritic and secondary fragment impact over long period of time”. Ouyang et al. (2005) summarized that, in broad definition, lunar regolith refers to any natural, space-weathered deposits on the lunar surface, but can be divided into three major categories: dust (particle diameter < 1mm), soil (particle diameter < 1 cm) and rock (particle diameter > 1 cm).

McKay, et al. (1991) summarized that, it is generally accepted that lunar maria regolith is around 4 – 5 m thick and 10 – 15 m thick at highlands, with the maximum depth considered to be 20 m. Such depth is enough to prevent the underlying bedrock being exposed and destroyed, as the impact flux has significantly decreased since 4 billion years ago. However, the depth of lunar regolith can still vary drastically depending on the site of study and methodology. Some examples include:

- 1) Theoretical studies: Based on observations reported by Oberbek and Quaide (1968), Oberbek, et al. (1973) used the Monte Carlo Method to suggest that areas with a higher number of impact craters should have thicker regolith.
- 2) Remote sensing: Bart, et al. (2011) examined the morphology of impact craters in 30 regions on both nearside and farside. Their results indicate the median thickness of lunar maria ranges at 2 – 4 m, and 6 – 8 m for lunar highland. Fa and Jin (2010) used the microwave radiometer on board the Chang’e-1 orbiter to measure the brightness temperature on the lunar surface. When inverted at the 3 GHz frequency, the average regolith thickness of Apollo mare sites was calculated to be 4.5 m thick, and highland at 7.6 m between the latitudes of 60 °N to 60 °S.
- 3) In-situ measurements: Seismograph stations that measured shear wave resonance at Apollo 11, 12 and 15 sites provided results of average thicknesses of 4.4, 3.7, and 4.4 m, respectively (Nakamura et al., 1975). The Chang’e-3 rover Yutu used ground-penetrating radar (GPR, or lunar-penetrating radar, LPR) at its landing site and determined the thickness of an ejecta layer up to 6 m, and a paleoregolith layer that reaches as deep as 11 m (Fa et al., 2015). Chang’e-4’s Yutu-2 rover had

revealed, also using an LPR, that its landing site on the lunar farside has a fine regolith layer as thick as 11 m, with an underlying coarser ejecta layer reaching down to 25 m (Lai et al., 2019). There is another layer underneath, believed to be fragmented basalt, for which Li, et al. (2020) had interpreted to be reaching as deep as 40 m.

Lunar regolith is shaped by space weathering, which includes a wide range of activities since the lunar surface is exposed to the space environment with almost no atmosphere. Such activities, illustrated in Figure 6, include meteorite and micrometeorite impacts, solar wind and cosmic radiation implantation (Taylor and Meek, 2005; Noble, 2009; McKay et al., 1991; Ouyang, 2005).

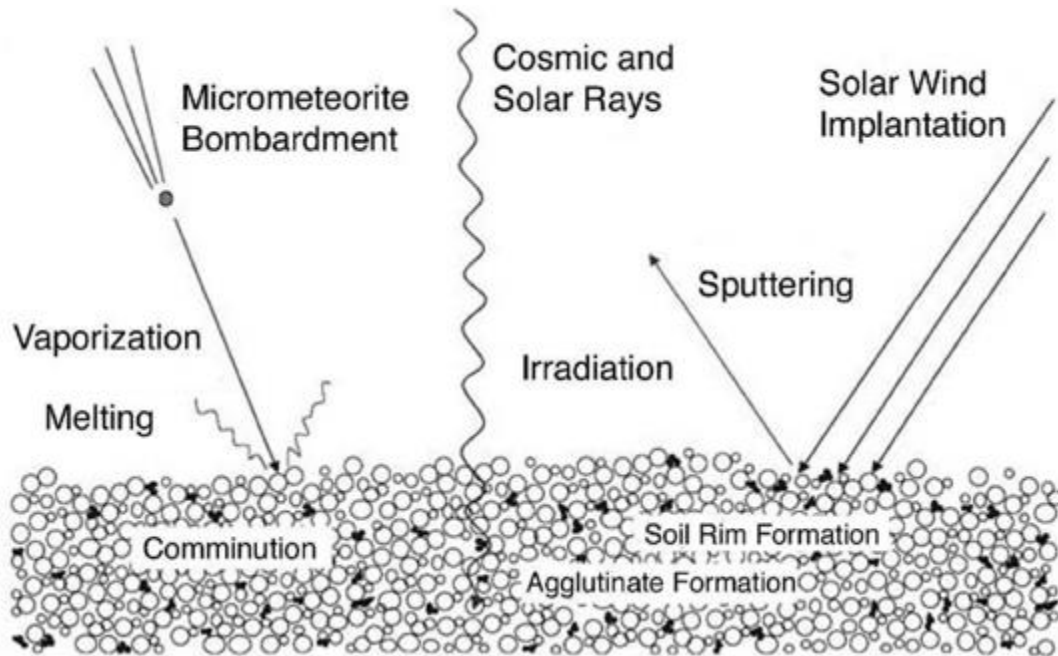


Figure 6. Space weathering processes that shaped regolith grains on the lunar surface (Noble, 2009).

Regardless of location on the Moon, returned samples of lunar regolith have shown consistent components that can be categorized into the following groups as found in Figure 7 (Ouyang, 2005; Noble, 2009; McKay et al., 1991):

- (1) Mineral fragments: grains of at least 80% of olivine, pyroxene, plagioclase, or ilmenite in composition;

- (2) Rock fragments: basalt, anorthosite, peridotite fragments;
- (3) Impact breccia and glass;
- (4) Agglutinates: unique component in the lunar regolith that are formed by impact glass bonding smaller grains together. They demonstrate complex shapes such as seen in Figure 8, and also can be found with nanometer-scale iron droplets (nanophase-iron, or np-Fe) on their surfaces.
- (5) Minor (<2%) meteoritic components from impact events;
- (6) Solar wind-implanted particles, such as hydrogen, helium-3, and noble gases.

The mixing proportion of each component is not fixed across the lunar surface, as demonstrated in Figure 9.

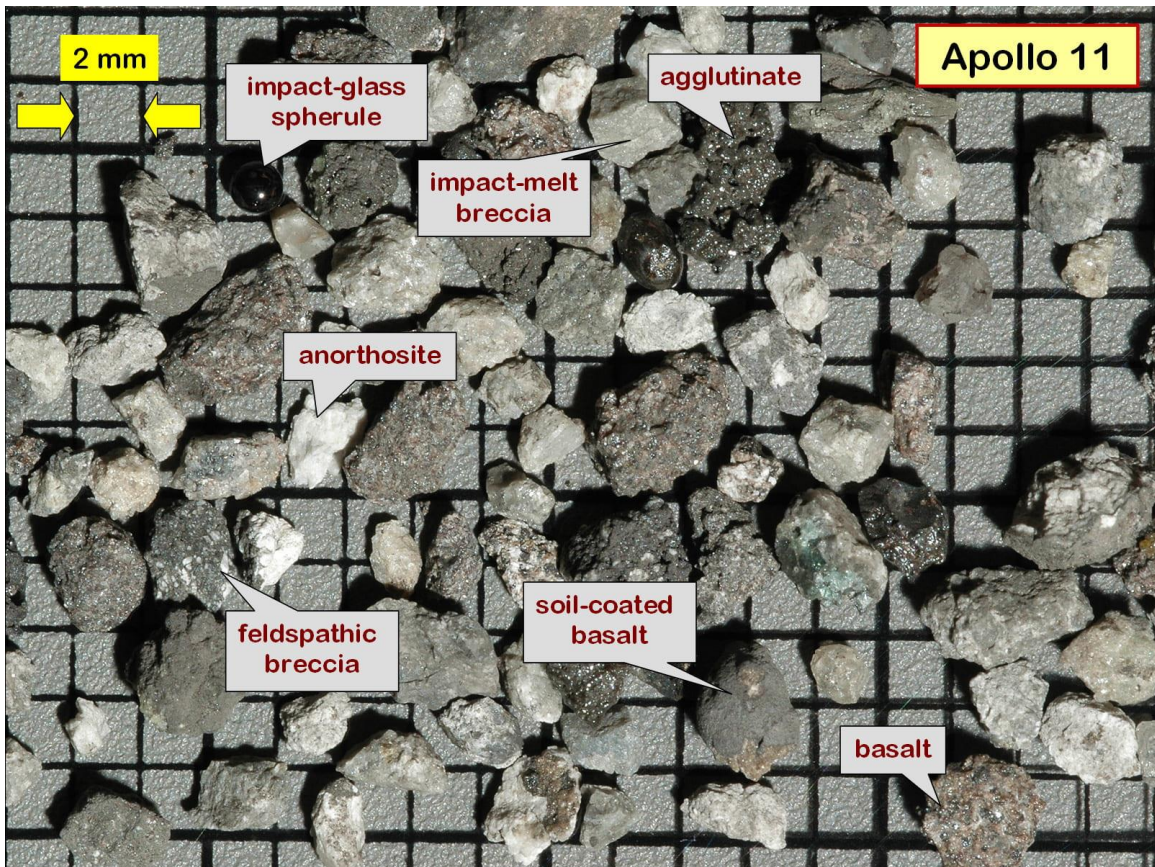


Figure 7. A portion of the rock fragments from Apollo 11 regolith sample, dominated by basaltic components as the mission was carried out at a lunar mare (Korotev, 2021).

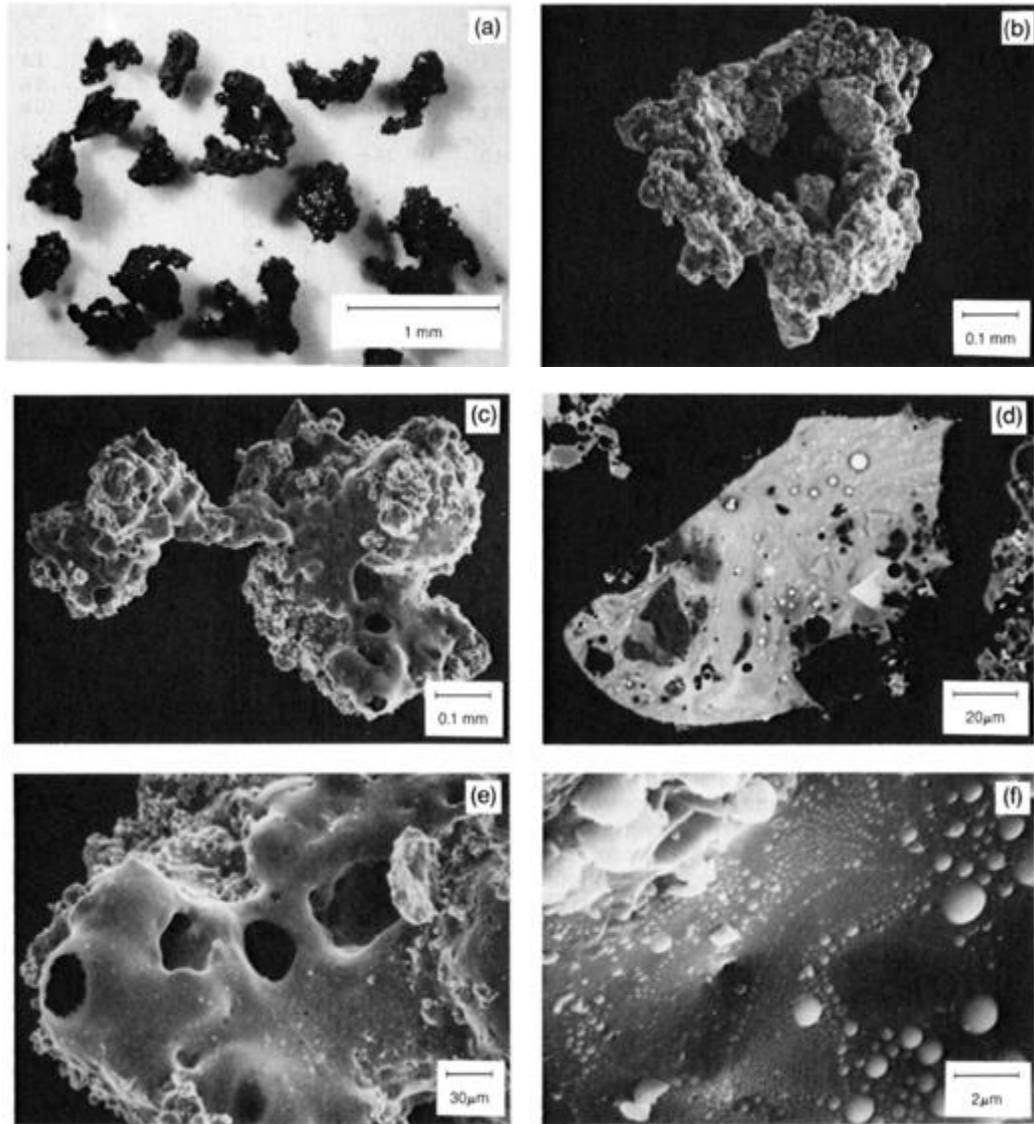


Figure 8. Close-up look of agglutinate particles that shows the irregular, porous, and ropey shape (a-e), as well as the np-Fe mounds on the surface of one agglutinate particle (f) (McKay et al., 1991).

There are a few ways to evaluate the surface exposure time of lunar regolith, also referred to as the “maturity”. In principle, lunar regolith is more mature as it receives more impact events and other space weathering processes, which indicates that finer grains and more agglutinates are expected in mature lunar regolith (McKay et al., 1991; Ouyang, 2005). Morris (1976, 1978) demonstrated that the ferromagnetic resonance (FMR) spectra of lunar soil normalized to the total iron content, which can be expressed as the I_s/FeO ratio, may

be a better tool of determining the exposure age. The main reason was that particle size and agglutinate percentage can be affected by the local bulk composition in addition to exposure age, where I_s/FeO is considered to only change with respect to exposure. Examples from Apollo 17 sample maturity variations are summarized in Figure 10.

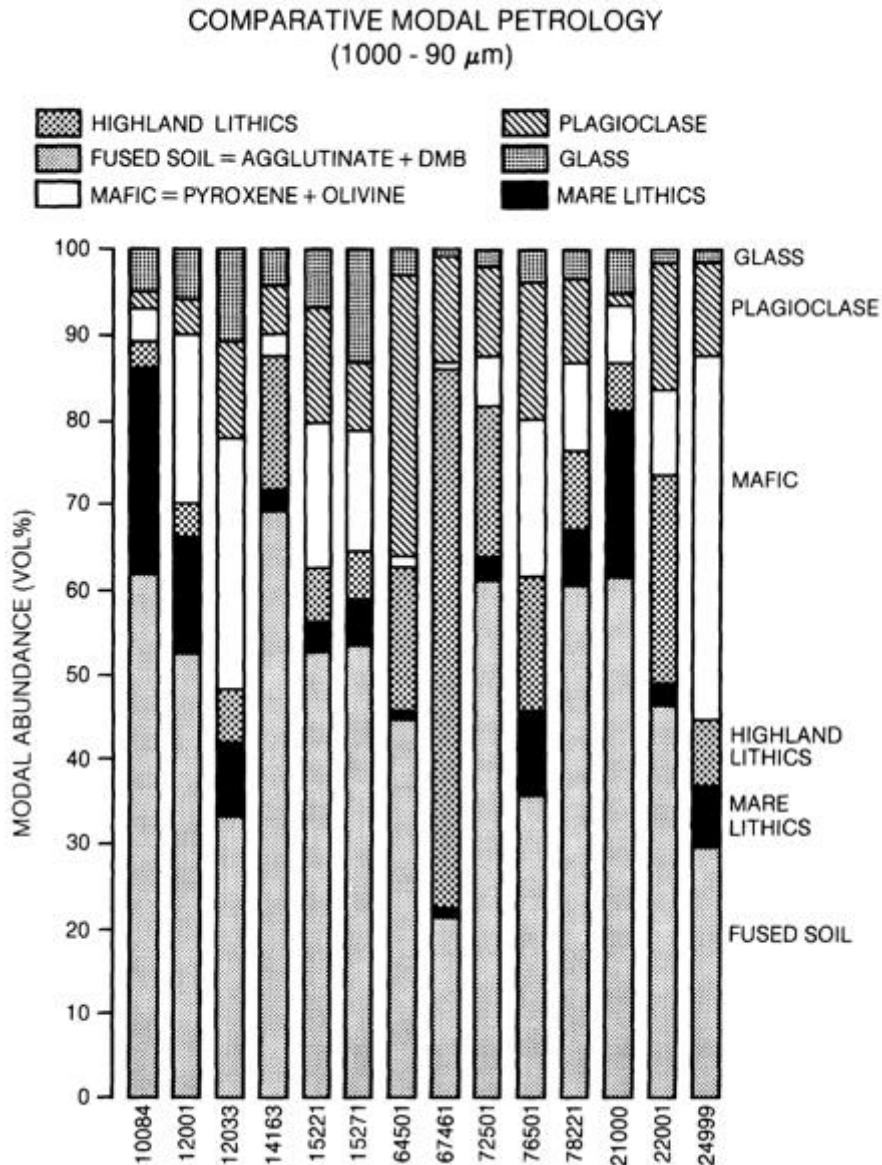


Figure 9. Lithic fragment composition of selected lunar regolith samples, except 24999 was from Luna 24 (Simon and Papike, 1981).

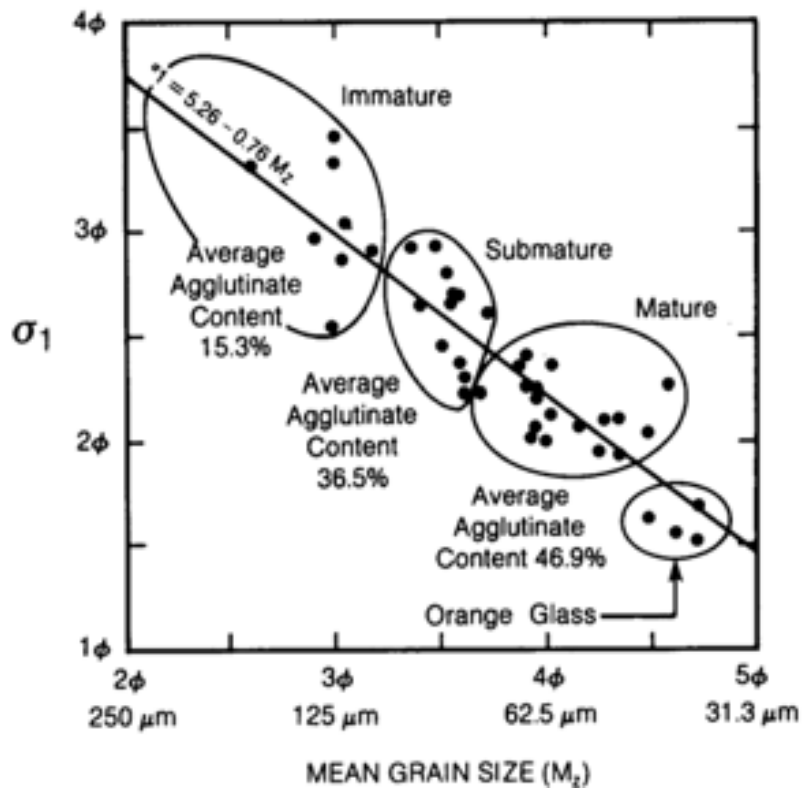


Figure 10. Sorting, grain size and agglutinate content relationship within 42 Apollo 17 regolith samples (McKay et al., 1991).

1.2.3 Physical and Geotechnical Properties

Since the evolution of lunar regolith largely involves mechanical break-downs, as well as radiation bombardment, loose regolith grains could display any type of particle shape, from completely spherical (e.g. glass spherules) to complicated (e.g. agglutinates) or angular (e.g. rock fragments) as seen in Figure 7, Figure 8 and Figure 11.

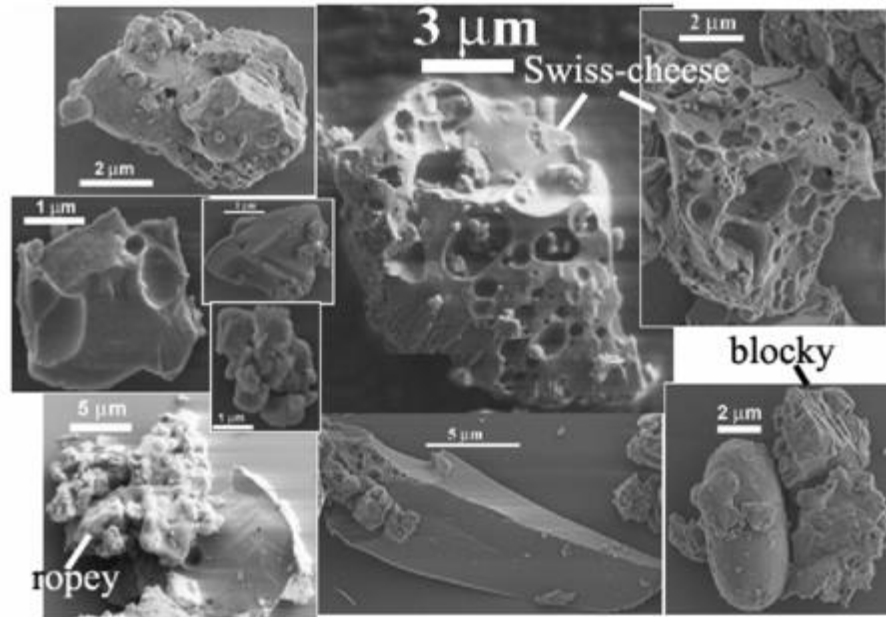


Figure 11. SEM images of Apollo 17 Sample 70051 dust particles, showing complex features such as the porous (“Swiss-cheese”) and “ropey” structures (Liu et al., 2006).

Lunar regolith is often described as “unconsolidated” because of its loose, poorly sorted nature (Carrier, Olhoeft and Mendell, 1991). Its particle size distribution could vary significantly from location to location. Figure 12 illustrated the differences of particle size distributions among several Apollo and Luna missions.

Lunar regolith is also known to be of higher specific gravity, ranging from 2.3 – 3.2, with 3.1 being recommended by Carrier, Olhoeft and Mendell (1991) for general engineering research (terrestrial soil specific gravity is around 2.7). Its average bulk density, is also higher than terrestrial soil, which are about 1.0 g/cm³ (sand), 1.3 g/cm³ (silt) or up to 1.6 g/cm³ (clay) (Rai, Singh and Upadhyay, 2017), where lunar regolith could be as dense as 1.5 g/cm³ even on the lunar surface (Carrier, Olhoeft and Mendell, 1991), as presented in Table 4 with porosity and void ratio values from 0 to 60 cm under the lunar surface.

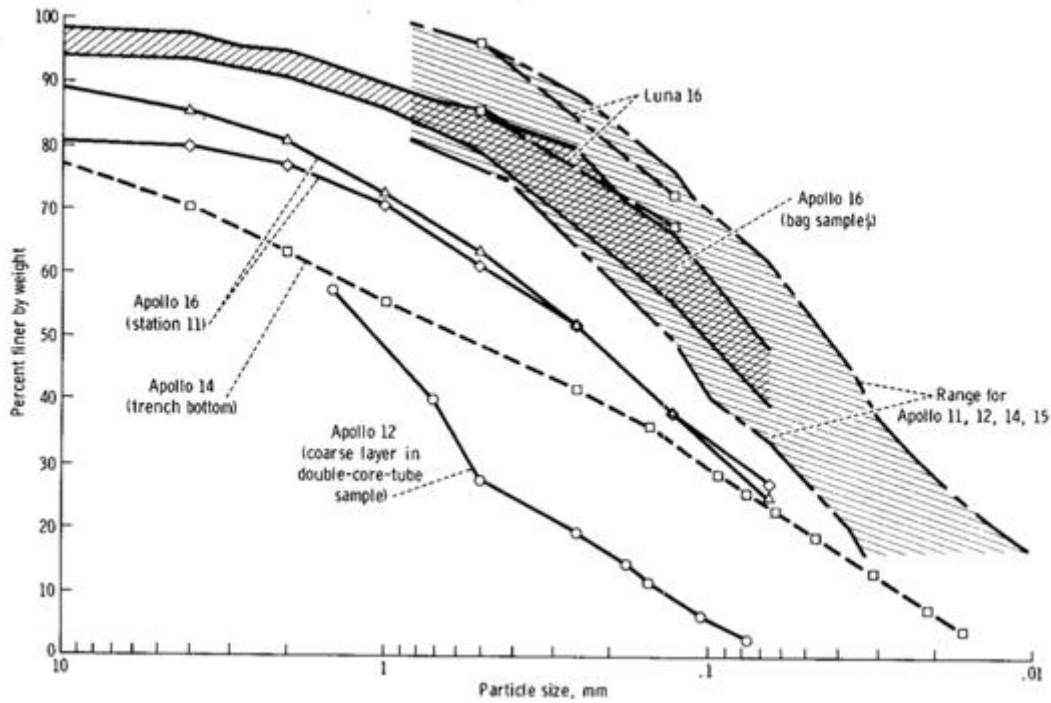


Figure 12. Particle size distribution among different Apollo and Luna landing missions (Mitchell et al., 1972).

Table 4. Lunar regolith average porosity, void ratio and bulk density at various depths (NASA, 2019; Carrier, Olhoeft and Mendell, 1991).

Depth Range (cm)	Average Porosity, n (%)	Average Void Ratio, e	Average bulk density (g/cm^3)	Relative density
0-15	52 ± 2	1.07 ± 0.07	1.50 ± 0.05	65 ± 3
0-30	49 ± 2	0.96 ± 0.07	1.58 ± 0.05	74 ± 3
30-60	44 ± 2	0.78 ± 0.07	1.74 ± 0.05	92 ± 3
0-60	46 ± 2	0.87 ± 0.07	1.66 ± 0.05	83 ± 3

1.3 Lunar Regolith Hazards and potential ISRU uses

Previous surface missions experienced challenges with lunar regolith, as its dusty nature and sharp grain shapes is significantly hazardous toward the safety and functioning of humans and equipment. Past missions have reported issues caused by lunar regolith, such as clogging machinery, abrade surfaces that come into contact, irritate eyes, skin and respiratory systems (Cain, 2010), and study also suggest that prolonged exposure to lunar regolith can even cause cancer (Caston et al., 2018).

However, lunar regolith is also considered to be a potential resource for ISRU as mentioned in Table 1. Researchers across the world have been developing technologies to demonstrate the feasibility of lunar ISRU, including but not limited to the following areas.

1. Lunar maria contains a very rich concentration of ilmenite, a mineral contains iron, titanium, and oxygen (FeTiO_2). Reducing ilmenite with agents such as hydrogen or methane could produce water, hydrogen, oxygen, iron and titanium for life support and manufacturing purposes. Examples studies: Jamanca-Lino (2021), Sargeant et al. (2020).
2. As the lunar surface has been constantly bombarded by space radiation, there is an estimated amount of 6.50×10^8 kg of helium-3 (^3He) globally. As seen in Figure 13, near side maria has a very high concentration (ppb/m²) but the far side has an intermediate concentration spread over a larger area. Despite having less thickness, the high concentration of ilmenite, an electro-conductive mineral, contributed to the better retention of implanted particles in the lunar maria (Shukla et al., 2020). Helium-3 is thought to be a clean nuclear resource that can be extracted for power generation. Example studies: Song et al., (2021), Fa and Jin (2007).

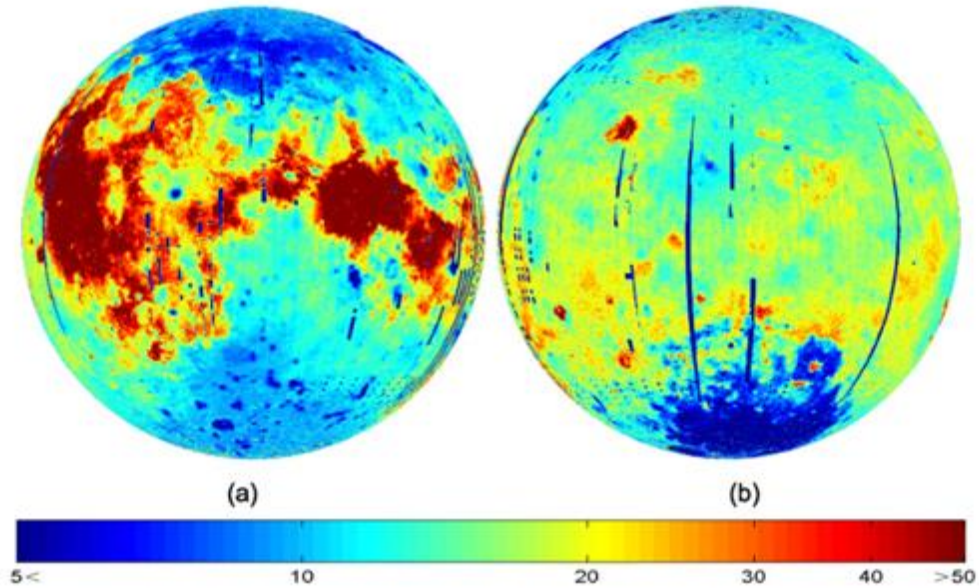


Figure 13. He-3 abundance on the near side and far side within the top 1 μm of lunar regolith, constructed with Clementine UV/VIS multispectral data (Fa and Jin, 2007).

3. Taylor and Meek (2004, 2005) found that lunar regolith could melt under microwave radiation. Microwave heating could provide a rapid and efficient solution to sinter regolith on the lunar surface, creating necessary infrastructures such as roads and landing pads for smooth traversing.
4. Various studies, such as Meurisse et al. (2018), De Kestelier et al., (2015), and Jakus et al., (2017) have been investigating the possibility to combine 3D printing with lunar regolith to produce construction materials for future lunar infrastructure.
5. Past missions such as NASA's LCROSS and ISRO's Chandrayaan-2 missions have detected hydrogen signature at the lunar poles, both sunlit areas and also in the bottom of some craters where sunlight cannot reach (Luchsinger, Chanover and Strycker, 2021; Spudis et al., 2010; Sridharan et al., 2010; Li et al., 2018). If the ice is proven exploitable, it will be a critical resource for life support systems that brings the first human settlement nearby.

1.4 Lunar Regolith Simulants and Their Limitations

To ensure safer and efficient future lunar surface missions, we usually need large quantities of regolith to test the new equipment. However, the quantity of lunar regolith returned to Earth is scarce to supply such demand. To solve this dilemma, researchers have attempted to create artificial lunar regolith using natural or synthetic terrestrial materials to replicate some critical properties of real lunar regolith, usually called “simulants”.

Regolith simulants are one of the most representative examples of a “functional analogue”, a term defined by Foucher, et al. (2021) as “*terrestrial sites, materials or objects exhibiting general prop-erties more or less similar to those anticipated on the targeted extra-terrestrial body, but having specific analogue properties that are highly or perfectly relevant for a given use*”. Functional analogues can be classified as analogue sites (large-scaled locations) and analogue samples (small-scaled objects). Although not perfect copies of their study targets, they have been used for many decades for various purposes and can be useful throughout the entire duration of a planetary exploration mission. Some examples and their limitations are presented in

Appendices

as summarized by Foucher, et al. (2021), followed by a diagram showing their relevance associated with each phase of a planetary exploration mission, from the conceptual and planning phase until evaluating the results after the end of the mission.

The first Workshop on Production and Uses of Simulated Lunar Materials in 1991 defined a simulant as “*Any material manufactured from natural or synthetic terrestrial or meteoritic components for the purpose of simulating one or more physical and/or chemical properties of a lunar rock or soil*” (McKay and Blacic, 1991). As of 2021, there are more than thirty documented types of lunar regolith simulants as of 2021 (i.e. see <https://simulantdatab.com/>).

Lunar regolith simulants (referred to as “simulants” hereafter) are usually produced by one of the following methods (after Jia et al., (2014)):

- 1) Select analogous materials on Earth, e.g. rocks that have similar geochemical/mineralogical composition to real lunar regolith. Process (e.g. crush and mill) into desired products. This method is faster and costs less when a large quantity is needed.
- 2) Introduce specific component(s) to products obtained from 1) to improve certain product properties. E.g. mix a denser material to increase product density. However this method may disturb some other stable properties, such as mechanical strength and overall uniformity.
- 3) Select specific minerals and mix according to desired proportions known from real lunar regolith. This method will produce mineralogically-accurate products, but can potentially raise the production cost and time, especially when producing larger quantities. Such products could be used to calibrate instruments and reach higher remote sensing data accuracy.

Simulants have provided convenience for a wide range of research topics, and counterpart products for Mars, asteroids and even comets were also developed and being improved over time. However, as the lunar regolith particles are complicated, space-weathered products, it is difficult to fully replicate every property within one simulant. In fact, most simulants serve just a few research purposes each. Some well-studied simulants (i.e. earliest models or most well-known products of a country or space agency) are listed in Table 5 as examples. Therefore, each simulant may be produced specifically to replicate just one or a few properties of real lunar regolith, such as particle size distribution, particle shape, density, and mechanical strength, and compromised on other properties that are not deemed critical or challenging to produce. This is commonly accepted especially in the cases when large quantities of simulants are expected.

Table 5. Examples of some lunar regolith simulants and their intended purpose(s).

Simulant name	Type	Country	Purpose	Reference
----------------------	-------------	----------------	----------------	------------------

JSC-1	Mare	USA	Large- to medium-scale engineering (e.g. material handling, excavation, transportation)	McKay, et al., (1994)
CAS-1	Mare	China	Microwave spectroscopy	Zheng, (2005)
EAC-1	Mare	Germany	Lunar surface simulation testbed	Engelschiøn, et al.,(2017)
FJS-1	Mare	Japan	Mechanical and thermal tests	Kanamori et al., (1998)
OB-1	Highland	Canada	Geotechnical tests	Battler and Spray, (2009)

Apart from technical limitations, financial challenges can also affect the quality of simulants. In a workshop report produced by LEAG and CAPTEM, Doug Rickman listed several factors that could affect the total cost of simulants, including the feedstock, design, production, evaluation and characterization, storage, shipping, and seeking consultation/advice (LEAG and CAPTEM, 2010). In addition, it is still not well known about the potential market for certain types of simulants, therefore developing a costly product may be risky at times.

Although these constraints will inevitably limit the possibility to produce simulants, it is also important for users to choose the appropriate type of simulants with minimum compromise.

1.5 Statement of Motivation

This thesis aims to characterize a set of lunar simulants to compare some of their fundamental properties. Specifically, the samples will address the role of mineralogy and shock deformation in simulants.

Cannon and Britt (2019) argued that, although most simulants focus on the bulk chemistry and physical parameters, not having the correct mineralogy could result in inaccurate outcomes when preparing for future lunar missions. Mineralogy would affect properties such as optical, geotechnical, magnetic and chemical reactivity, and therefore impact several ISRU research topics, including melting regolith, extracting oxygen and metals, and creating ceramics or other composites (Cannon and Britt, 2019; Landsman, 2020). In this study, a new type of simulant with lower mineralogical fidelity was created and compared with an existing simulant that is more mineralogically accurate.

In addition to mineralogy, another factor that affects the mechanical and geotechnical strength of lunar regolith grains is that they are fractured and weakened from impact shock events on the lunar surface (Allton, Galindo Jr. and Watts, 1985). Mineralogy and grain strength may affect the durability of terrestrial infrastructure. Sadrekarimi and Olson (2008) presented that, having more compressible minerals with weaker shear strength often lead to liquefaction failure, but it is not yet known if lunar infrastructures built from lunar regolith will be affected. Shocked nature in simulant grains was categorized as “cannot yet produce” in Appendix E but has been rarely attempted and its importance to be included in lunar simulant is not widely discussed. One of the very few documented attempts of producing shocked simulant particles to date was Boslough et al. (1992)’s attempt of generating shock wave using explosives on the Minnesota Simulant Lot 2. Such procedure is costly and potentially dangerous, and more difficult control the outcome of the product properties. In this study, a new type of simulant was produced as an attempt to create shocked grains and compared with the other two products on their fundamental properties.

Based on the comparison results, this study will provide some input on whether shocked grains were successfully created, and comment on the how the simulants’ behaviours were affected by mineralogical fidelity and shocked nature. Regardless of the outcomes, this study aims to contribute to the discussion on the significance of shocked grains and mineralogical accuracy within lunar simulants, as well as to provide some educational value on the importance of producing and choosing the best type(s) of simulant based on specific research purposes.

The following chapter will introduce and describe these simulants that are selected for this study, as well as the properties examined, and the methods used for characterization.

Chapter 2

2 Methods

This chapter describes the samples used for analyses and the techniques used to process and characterize all simulant samples. Each property being analyzed will be briefly explained with its importance in lunar simulants.

A total of three types of lunar highland simulants as introduced in Table 6 and later described in Section 2.1 are used for this study, two of which were created at the University of Western Ontario using different sources of feedstock (i.e. the original, root material(s) used to make the simulants).

Table 6. General information of samples used in this study.

Name	Producer	Feedstock	Note
LHS-1	CLASS Exolith Lab, USA	Mineral mixture	Commercially available, focuses on mineralogy
UWO-1S	Author of this study	Impact rocks from Mistastin Crater, New foundland and Labrador, Canada	Original simulant, attempted to create shocked grains
UWO-1G	Author of this study	White Mountain anorthosite “Greenspar” from Greenland, provided by Hudson Resources, Inc.	Original simulant, not focused on mineralogical accuracy (i.e. no additional components other than anorthosite is included) or shocked grains, but may serve mechanical tests as a component of a simulant product.

2.1 Sample description

This section introduces the samples used for this study, including the geological background of the feedstock and preparation methods will be described where applicable. All simulants only simulate the common mineral and rock grains, with no agglutinates, np-Fe, and other components described in Section 1.2.2 added.

2.1.1 LHS-1 by Exolith Lab

The LHS-1 (Lunar Highland Simulant) simulant (Figure 14) is a simulant created by the Exolith Lab, an organization largely funded by the University of Central Florida (UCF)'s Center for Lunar & Asteroid Surface Science (CLASS) from the USA (Cannon and Britt, 2019). Exolith Lab specifically focuses on mineralogical composition in their products, which includes lunar, Martian and asteroidal simulants. For lunar simulants, agglutinates and dust simulants are also currently available as separate products. The production of LHS-1 corresponds to the 3rd method described in Section 1.4, where mineral and rock fragments are mixed in proportion (Exolith Lab, 2021).

At the time of this study, LHS-1 is produced to simulate the generic lunar highland regolith (Exolith Lab, 2021), contrary to some simulants that are based on samples collected from a specific mission (e.g., CAS-1 and FJS-1 were made based on Apollo 14 sample average) (Zheng, 2005; Kanamori et al., 1998) or one specific sample (e.g., JSC-1 was made to simulate Apollo 14 sample 14163 and OB-1 was made to simulate Apollo 16 sample 64500) (McKay et al., 1994; Battler and Spray, 2009).



Figure 14. LHS-1 lunar highland simulant from the Exolith Lab.

Other well-simulated properties, as claimed on Exolith Lab's website (<https://exolithsimulants.com/pages/simulant-introduction/>), include particle size distribution, volatile release (for Martian and asteroidal simulants). Additionally, although not intentionally targeted, the high mineralogical fidelity can also lead to better reflectance spectra data and magnetic ability. However, just like any other simulant, some other properties are compromised in Exolith's products. The lab has thus indicated that particle shapes (not angular enough for lunar simulants), trace elements, hazardous components (e.g. perchlorate in Martian simulants) and reactivity (when exposed to terrestrial atmosphere) are not meant to be very accurate. Another inevitable inaccuracy comes from the fact that, since all materials were obtained from natural terrestrial sources, weathering processes in the minerals could lead to excess or deficiencies in some elements, such as Mg, Na, K, Fe and Ca. Nanophase iron in lunar regolith is also not simulated at the time of this study.

Table 7. Mineralogical composition as mixed of LHS-1 as indicated on its product datasheet (Exolith Lab, 2021).

Component	Weight %
Anorthosite	74.4
Glass-rich basalt	24.7
Ilmenite	0.4
Olivine	0.3
Pyroxene	0.2

2.1.2 Original simulant UWO-1S

UWO-1S was created as a new attempt to produce shocked grains. As introduced in Section 1.5, previous attempts in creating shocked grains in lunar simulants were all based on the procedure of artificially shocking the simulants, which could be very costly to produce even small amounts. In this study, a novel attempt to create shocked grains of simulants was carried out, to pulverize impact rocks into fine grains.

2.1.2.1 Feedstock source

The feedstock used to create UWO-1S were collected from the Mistastin Crater (Figure 15), located in the province of Newfoundland and Labrador in eastern Canada. The Mistastin Crater shows an unusual elliptical shape, depression towards the east/northeast direction, and was the second crater in Canada whose approximate location was predicted before being discovered (Currie, 1968).

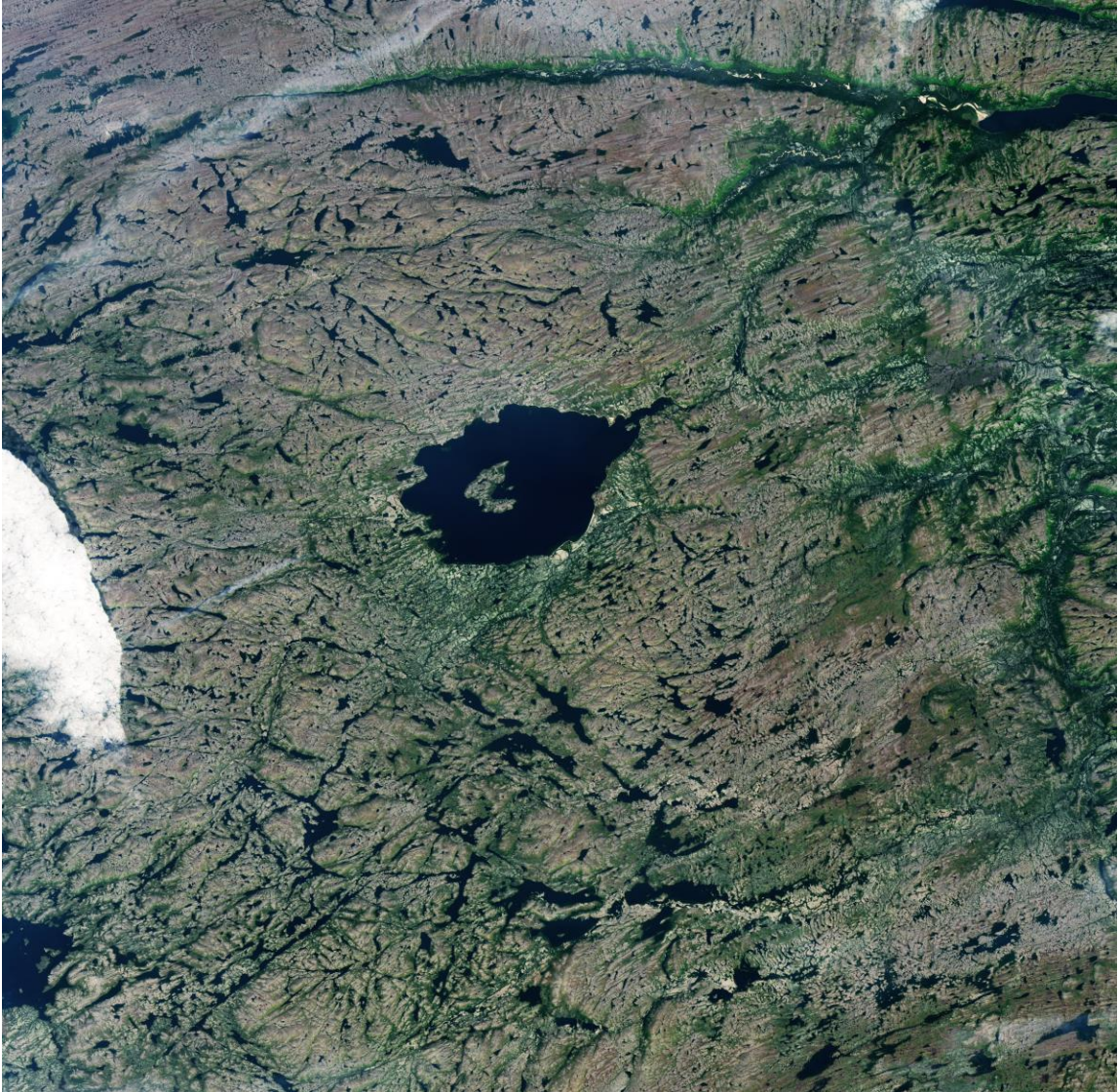


Figure 15. Satellite image of the Mistastin Crater from the Landsat 8 Operational Land Imager, taken in September 2017 (NASA Earth Observatory, 2017).

The crater is believed to have formed around 36 million years ago and spans about 28 km in diameter with a 16-km crater lake in the center (Marion and Sylvester, 2010; Mak et al., 1976). Past field examinations concluded that the petrological compositions in this crater include anorthosite (54-71%), some mangerite (around 14%) and granodiorite (14-33%) (Grieve, 1975; Marion and Sylvester, 2010). Petrographic distributions of these compositions are illustrated in Figure 16, and a formation diagram of the crater can be found in Figure 17.

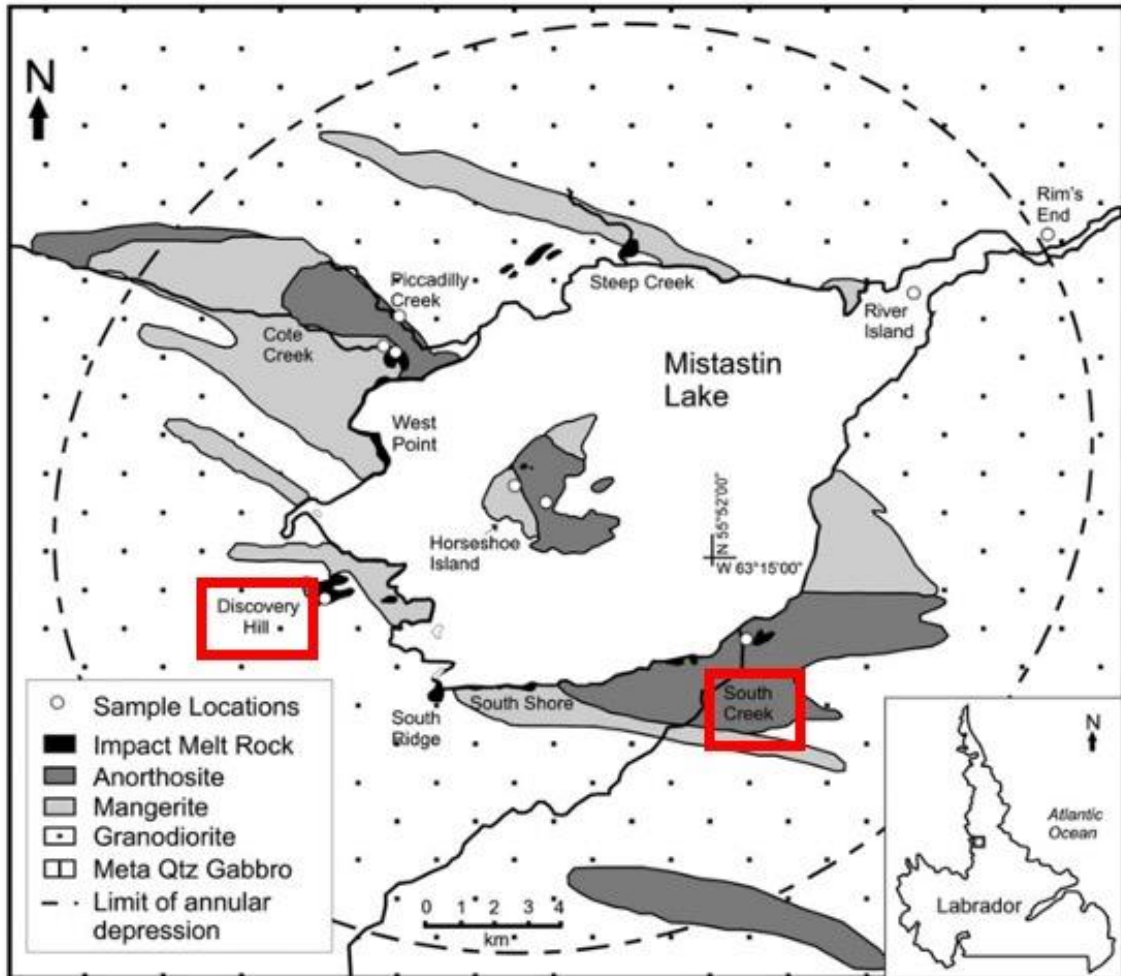


Figure 16. Geologic map of the Mistastin Crater. Red boxes indicate the locations South Creek and Discovery Hill where the feedstocks were collected from. Bottom right: Location of the crater in Labrador, Canada. Modified from Pickersgill, Osinski and Flemming (2015), based on previous studies of Marion and Sylvester (2010), Grieve (1975) and Currie (1971).

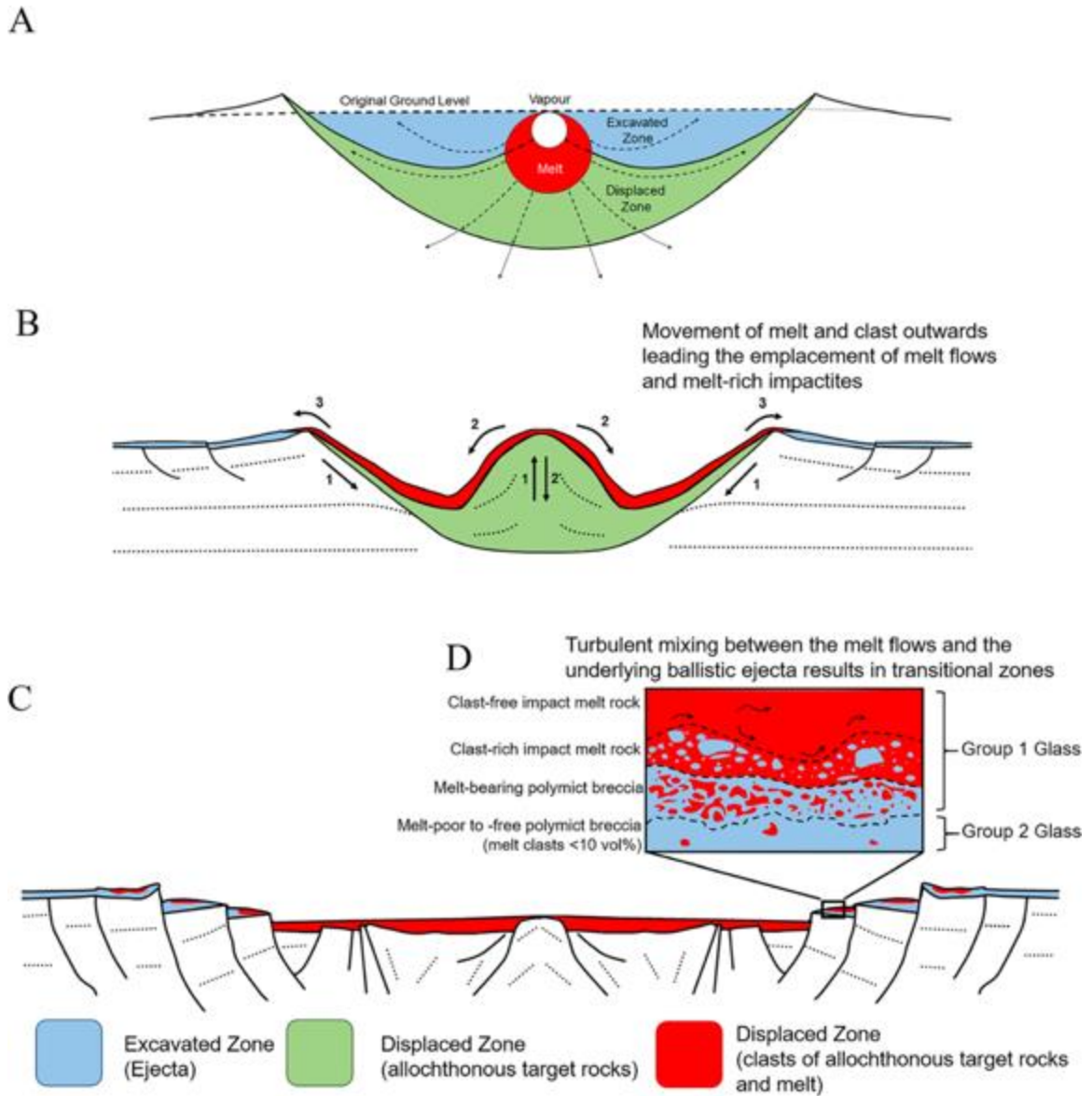


Figure 17. Formation process of the Mistastin Crater (Hill, Osinski and Banerjee, 2020) .

The UWO-1S simulant contains two major components. The first one is anorthosite-rich, polymict breccia sourced from South Creek (Figure 18). The breccias have fine-grained matrix with glass and poorly sorted lithic clasts. Mader and Osinski (2018), Hill, Osinski and Banerjee (2020) had stated that the breccia within the crater exhibits a wide range of shocked features, indicating various shock levels from 0 to 60 GPa. Thin sections obtained from the rocks used as feedstock have also demonstrated various shocked features as seen

in Figure 19, with planar deformation features (PDF) and melting crystal boundaries were observed.



Figure 18. Examples of An-rich breccia from South Creek.

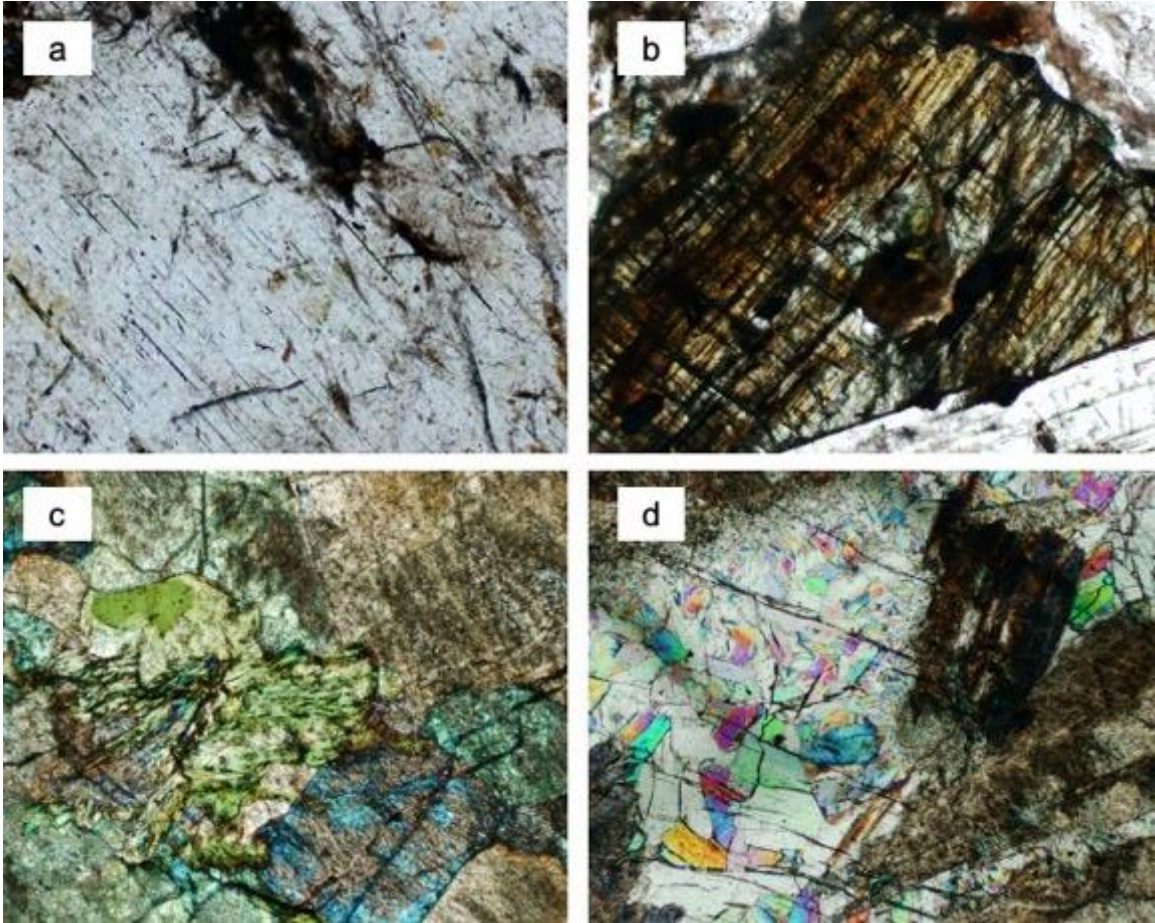


Figure 19. Thin section images of an anorthosite breccia used to create UWO-1S. PDFs (a, b) and melting grain boundaries (c, d) could be observed, confirming the description in Hill, Osinski and Banerjee (2020). In addition, irregular fractures can also be observed in all images.

The other component is clast-poor to clast-free impact melt rocks, also collected from the Mistastin Crater at the Discovery Hill (Figure 20). The rocks are of grey colour, with very fine-grained matrix. Figure 21 shows some shocked features of the melt rocks through observing the thin sections. Hill, Osinski and Banerjee (2020) also concluded that the shock level on these melt rocks can be at 60 GPa.



Figure 20. Examples of the melt rocks from Discovery Hill, used to create UWO-1S.

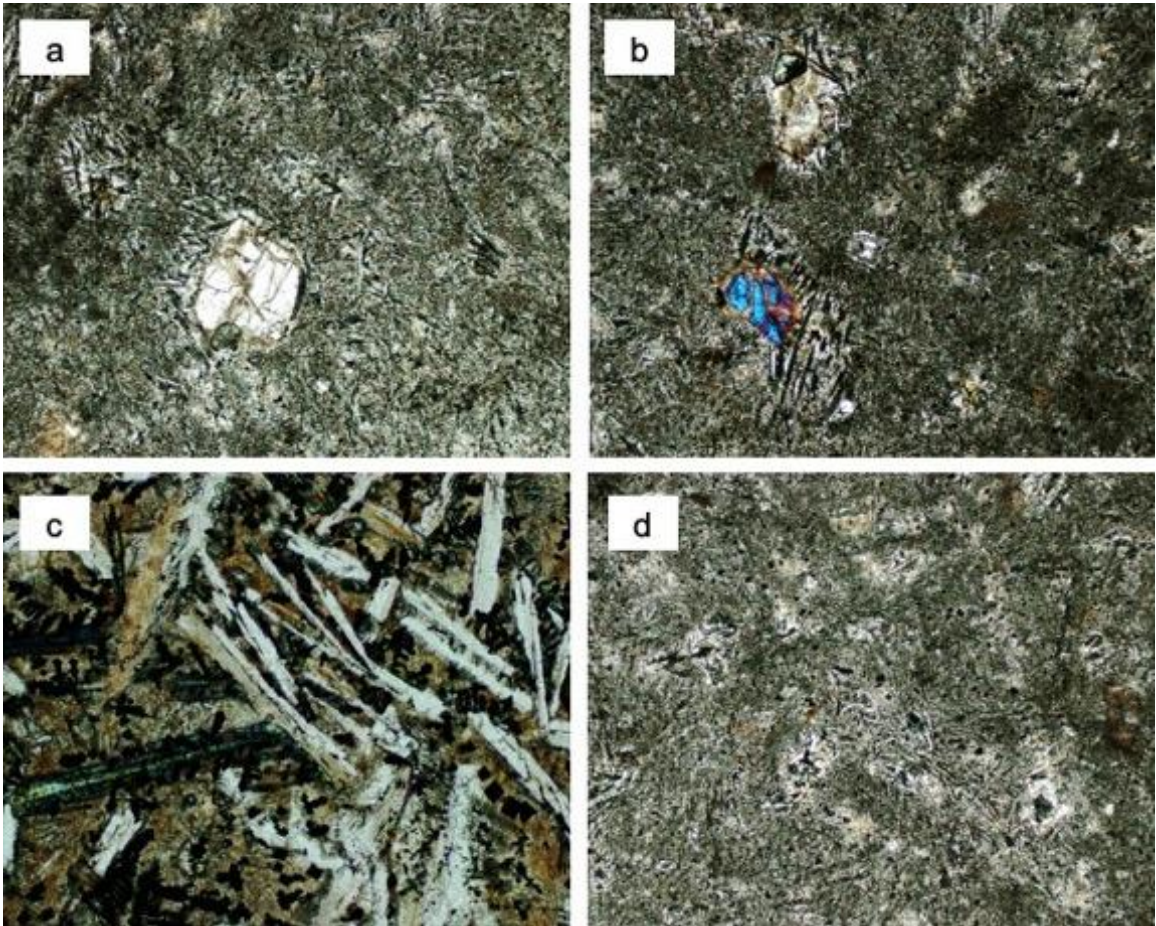


Figure 21. Thin section images of an impact melt rock used to create UWO-1S. (a), (b) and (d) can be seen with fine-grained groundmass with small crystals or glassy components. Impact crystalline features are seen in (c).

2.1.2.2 Processing steps

The most conventional way of preparing lunar simulant samples from whole rocks is to crush them into small fragments and then grind with one of a few steps will milling equipment. Some examples are described in Table 8.

Table 8. Examples of milling steps applied to produce lunar simulants in large quantities.

Simulant	Country	Feedstock	Processing steps	References
KLS-1	Korea	Basalt from Cheorwon	Crushing with jaw crusher, hammer mill grinding, screening and sieving to match the desired result.	Ryu, Wang and Chang, (2018)
OB-1	Canada	Archean anorthosite from Shawmere, Ontario	Using jaw crusher, roll crusher, and ring crusher to break down feedstock into coarse, medium and fine grain size fractions.	Battler, M. (2008)
FJS-1	Japan	Basalt from Mt. Fuji	3 types of crushers/mills to break down feedstock to coarse, medium and fine grain sizes.	Kanamori et al., (1998)
LSS-ISAC-1	India	Anorthosite from Sittampundi Anorthosite Complex	Manual and mechanical (e.g. ball milling) grinding of feedstock into different particle size ranges.	Venugopal et al. (2020)

Due to COVID-19 pandemic restrictions, the simulants created for this study were created using available equipment within the Department of Earth Science at UWO, at the Thin

Section Lab with a chipmunk crusher from Bico Inc., and a vibratory ring pulverizer from T.M. Engineering Ltd., as shown in Figure 22.



Figure 22. Bico Chipmunk Crusher (Left) and T.M. Vibratory Ring Pulverizer (Right).

As illustrated in Figure 23, the rocks were first crushed into small fragments using the crusher, then transferred into the pulverizer container in small batches, filling approximately 1/3 of the container, and ground into fine-sized grains. The time for each grinding session depended on the amount of rock fragments added to the container and the hardness of the material. The breccias required at least 60 seconds each batch, sometimes an additional 15-20 seconds were needed. The melt rocks were easier to be ground, where 40-60 seconds were sufficient. Before pulverizing the melt rock fragments, all identifiable clast fragments were removed. The finished breccia and melt fines are presented in Figure 24.



Figure 23. Rocks (impact melt rocks pictured) were tossed into the Bico crusher (upper left) and crushed into smaller masses (upper right), then transferred into the ring pulverizer container (lower left) to be ground into powder-like product (lower right).

After grinding, the product was sifted through a stack of sieves to determine their particle size distribution, which will be described in Section 2.3, and then adjusted to fit the target range. Both breccia and melt rocks are commonly found in returned Apollo samples, with melt taking up to 50% in soil samples, 30-50% in highland hand specimen rocks (Ryder,

1981; Hörz et al., 1991). For this study, each component was characterized individually, and mixed for a 1:1 ratio for the same set of characterizations as a trial.



Figure 24. Pulverized breccia (left) and melt rock (right).

2.1.3 Original simulant UWO-1G

The feedstock of the UWO-1G produced for this study is the Greenland “White Mountain” Qaqortorsuaq Anorthosite, nicknamed “Greenspar”, mined and provided by Hudson Resources Inc. from the White Mountain Anorthosite Project. The Greenspar (Figure 25) provided by Hudson Resources is a granular state and mostly white in colour.



Figure 25. Greenland anorthosite "Greenspar" provided by Hudson Resources Inc., before processing.

With over 90% plagioclase feldspar in the anorthosite and a high An number of 83, the Greenspar is a major component of LHS-1 (Landsman, 2020; Exolith Lab, 2021), and is also being proposed as a potential component as a future lunar polar simulant, such as mixing with ice to simulate the polar ice regions, or as-is (Gruener et al., 2020).

As described in Section 1.4, the first two methods of simulant production are more common due to less cost and time, especially when large quantities are needed. Some examples

include OB-1 (Shawmere anorthosite and olivine slag) (Battler and Spray, 2009), OPRH2N (Shawmere anorthosite and basaltic cinder) (Zhang et al., 2019), NAO-1 (gabbro from the Yarlung Zangbo River) (Li, Liu and Yue, 2009), and TUBS-T (Scandinavian gabbro complex) (Linke et al., 2020). However, such products will also have lower mineralogical fidelity and therefore may behave differently compared to simulants that are more mineralogically accurate (but more costly and time-consuming to produce), as stated by Cannon and Britt (2019). To address the question on how mineralogical fidelity affects simulant behaviours, UWO-1G was created with only Greenspar to represent a simulant with lower mineralogical accuracy and compare with LHS-1, a simulant that is more mineralogically accurate but contains the same anorthositic feedstock.

2.1.3.1 Feedstock source

Greenland is the largest island on Earth, composed of several geological terrains that date from 3.9 Ga to 390 Ma, but over 80% of the area is covered by ice (Dawes, 2009; White et al., 2016). The mining location of Greenspar, an Archean-origin anorthosite, is said to be approximately 85km southwest from the town of Kangerlussuaq (Gruener et al., 2020), marked by the red arrow in Figure 26.

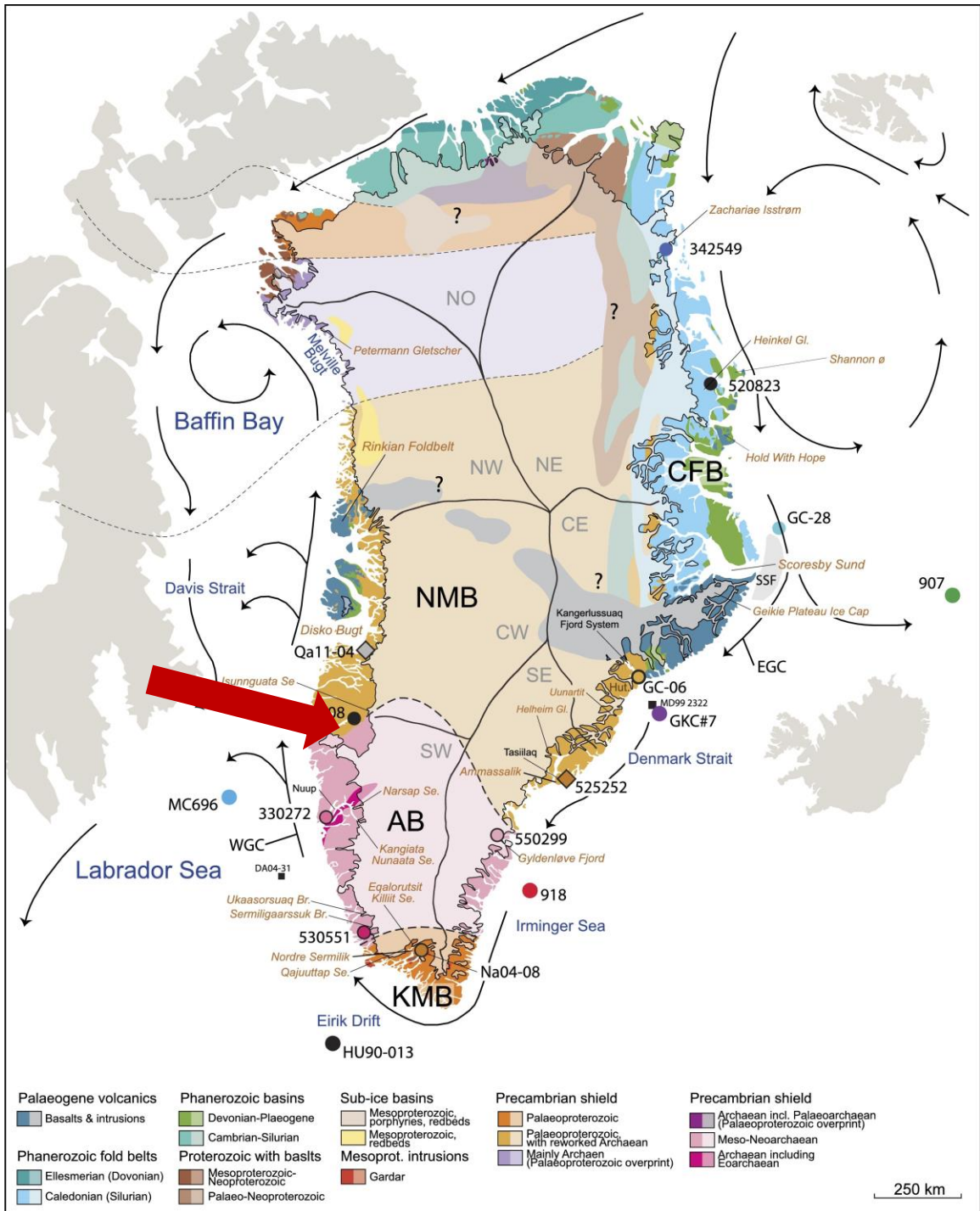


Figure 26. Geologic map of Greenland (White et al., 2016). Red arrow indicates the approximate location of the White Mountain Greenspar mining site.

2.1.3.2 Processing

For this study, the Greenspar anorthosite sample was processed with the same pulveriser for this study in order to match the particle sizes with LHS-1 and UWO-1S for comparison. Same as processing the Mistastin impact rocks, small quantities of the Greenspar were added to the pulveriser container and ground for at least 40-60 seconds each time. The final product, as shown in Figure 27, was sieved using the same settings as the Mistastin impact rocks and adjusted to meet the target particle size distribution range.

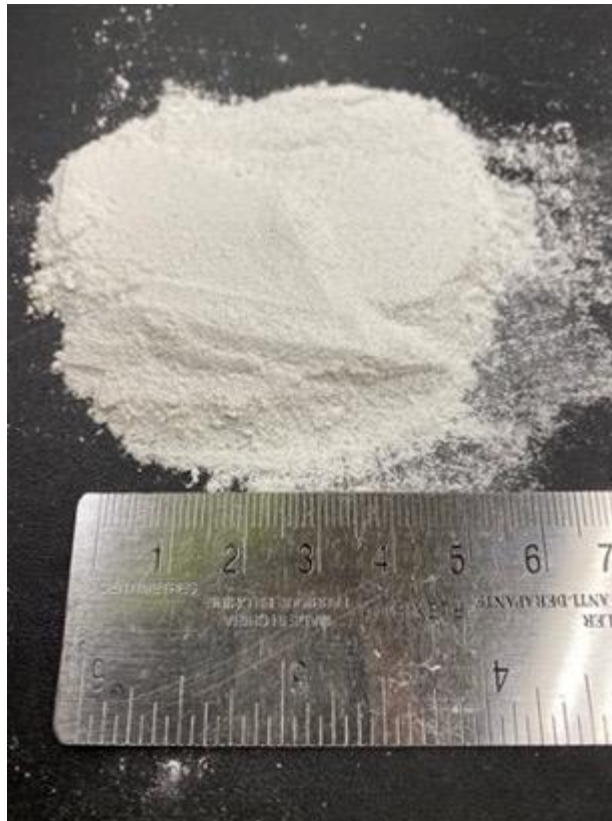


Figure 27. Finished product of UWO-1G.

2.2 Particle Shape

Rickman, et al., (2012) listed several physical and mechanical properties that will be affected by lunar regolith particle shapes, including strength, repose angle, packing density, how particles will attach, abrade, and clog machinery on the lunar surface. Therefore,

simulants used for relevant research should simulate appropriate particle shapes to ensure the quality of future space hardware that will come to contact with lunar regolith directly.

To image individual particle shapes under a smaller scale, all simulants were sent for Scanning Electron Microscope (SEM) at the Department of Physics and Astronomy at UWO, with a LEO (Zeiss) 1540 Focused Ion Beam (FIB)/SEM instrument.

2.3 Particle Size Distribution

In an unconsolidated soil, such as lunar regolith, the particle size distribution would control multiple factors that affect its physical properties, notably their compressibility, optical, thermal and seismic performances (Carrier, Olhoeft and Mendell, 1991). For this reason, the simulants used for this study were aimed to closely match with each other to allow the subsequent comparison.

All simulants were sifted through a stack of sieves at the Department of Civil Engineering to determine their particle size distribution (PSD). The number of each sieve and their sizes can be found in Table 9, in the order from top to bottom. However, this method only allows the characterization of particles greater than 75 μm . Finer grains were collected onto the bottom pan of the sieve stack, and about 50g of this portion was taken for further PSD analysis using a hydrometer.

Table 9. Number and sizes of the sieves used to characterize PSD for this study.

Sieve number	Sieve size (μm)
4	4750
16	1180
35	500
80	180
100	150
120	125
140	105

200	75
Pan	N/A



Figure 28. (Left) Assembled sieve stack; (Middle) Sample (UWO-1G pictured) added from the top (No. 4) sieve; (Right) Stack placed into a mechanical shaker to sift for 12 minutes.

Since the simulants are intended to be compared together for physical properties, the two original simulants were intended to match with the PSD of LHS-1, which is the average PSD of lunar highland samples brought back from the Apollo missions.

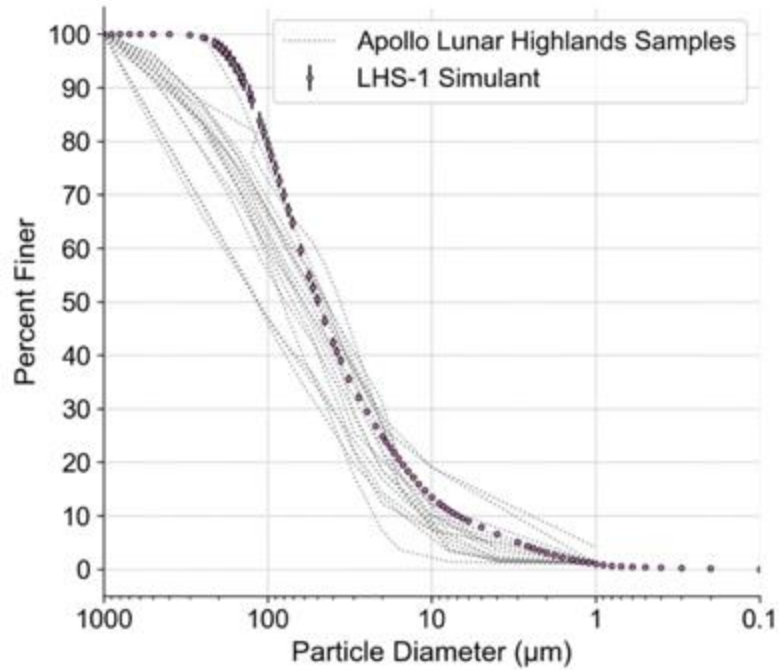


Figure 29. LHS-1 Particle size distribution as provided on the product fact sheet (Exolith Lab, 2021).

The hydrometer test is based on Stoke’s Law to measure the terminal velocity of different particle sizes falling in a stationary solution, where the terminal velocity is proportional to the squared value of the particle diameter, assuming all particles are spherical (ASTM International, 2017). As illustrated in Figure 30, to prepare for the hydrometer test, about 40g of sodium hexametaphosphate ($\text{Na}_6[(\text{PO}_3)_6]$) was thoroughly dissolved into 1L of distilled water in a graduated cylinder. The solution, called a deflocculating agent, prevents fine particles to clump together and therefore affect the sedimentation result (Kaur and Fanourakis, 2016). 125ml of the deflocculating agent was then added to the pre-measured sample fines (around 50g) to be mixed, and each mixture was set aside for at least 8 to 12 hours before characterization.

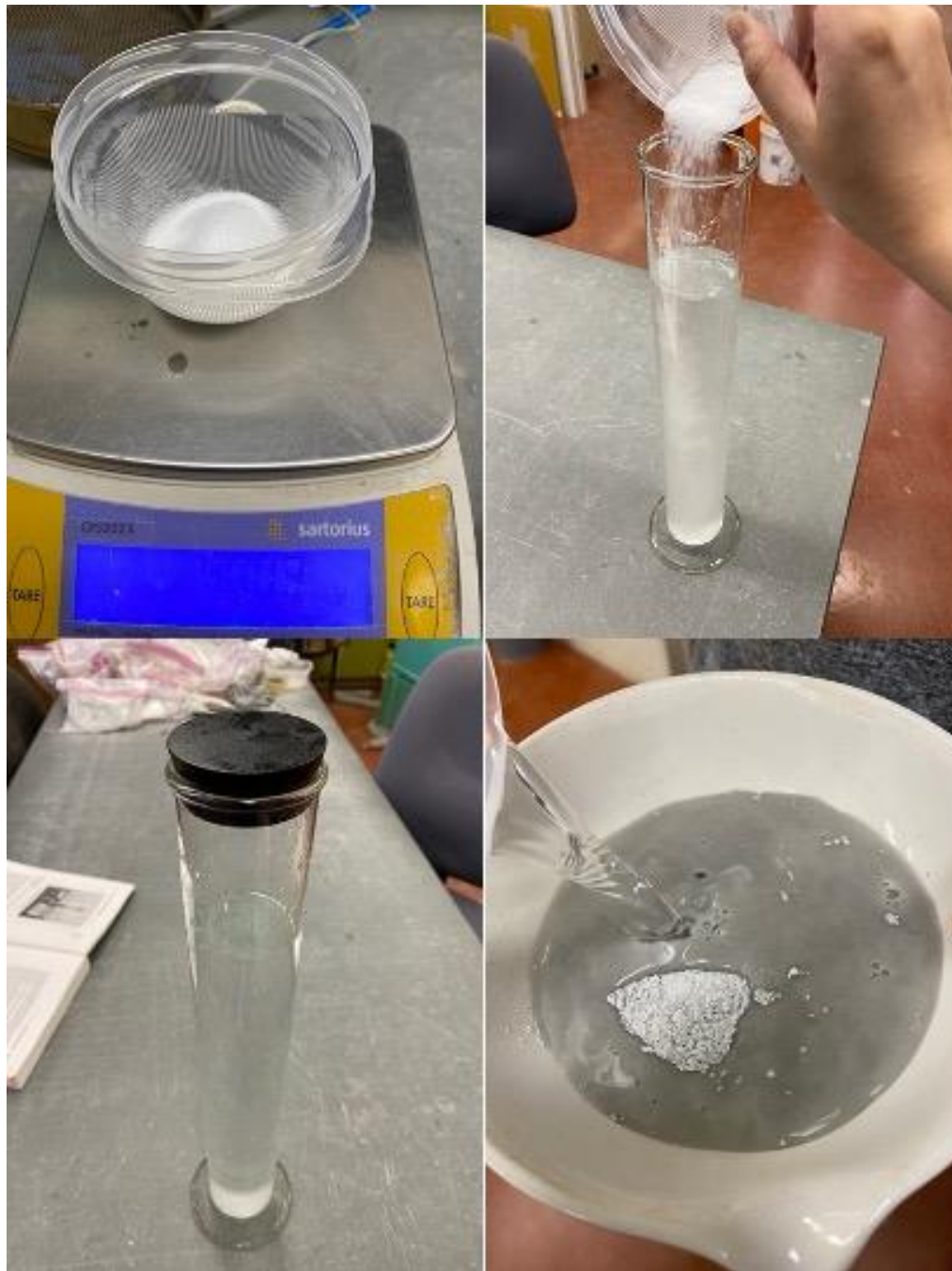


Figure 30. Preparing for hydrometer test. 40g of sodium hexametaphosphate was weighed (upper left), and then added to 1L of distilled water (upper right). The container was then sealed and shaken to dissolve the solid (lower left) and the final solution was added to around 50g of the sifted fines (lower right, LHS-1 pictured).

To initiate characterization, 125ml of the deflocculating agent was added to 875ml of distilled water in a new graduated cylinder and measured for temperature. An ASTM-152H soil hydrometer was then carefully placed into the cylinder for obtaining an initial reading F_z . The sample mixture was then transferred to a mixer cup, with all residues rinsed with distilled water, and stirred for 1 minute with an electric mixer. When stirring is completed, the mixture was poured into another clean graduated cylinder and filled to the 1L mark with distilled water. After sealing the cylinder with a rubber stopper and shaken well, the hydrometer was then placed into the liquid immediately for reading. Data was recorded at the following time marks (counted from the beginning of the measurement process): 15s, 30s, 1min, 2min, 4min, 8min, 15min, 30min, 1h, 2h, 24h and 48h.

The results from both sifting and hydrometer tests were plotted separately first, then combined to generate a full PSD for each sample.

2.4 Mineralogy Identification

As this study compares highland simulants, the major component expected in all simulants is plagioclase feldspar, which is the predominant component in anorthosite (Table 10).

Table 10. Plagioclase mineral group (Haldar, 2020).

Plagioclase mineral	An% (% of $\text{Ca}(\text{Al}_2\text{Si}_2\text{O}_8)$)	Ab% (% of $\text{Na}(\text{AlSi}_3\text{O}_8)$)
Anorthite (An)	90-100	0-10
Bytownite	70-90	10-30
Labradorite	50-70	30-50
Andesine	30-50	50-70
Oligoclase	10-30	70-90
Albite (Ab)	0-10	90-100

As illustrated in Figure 31, Lunar anorthosite has a high-An composition, being predominantly (i.e., $>An_{90}$) anorthite, while terrestrial anorthosite might vary from maximum An_{90} to An_{40} or lower (Papike, Taylor and Simon, 1991; Wood et al., 1970; Ashwal and Burke, 1987). Gruner et al. (2020) have shown that Greenspar has an An number of ~ 84 , which means that both UWO-1G and LHS-1 should have at least bytownite and anorthite as the major components.

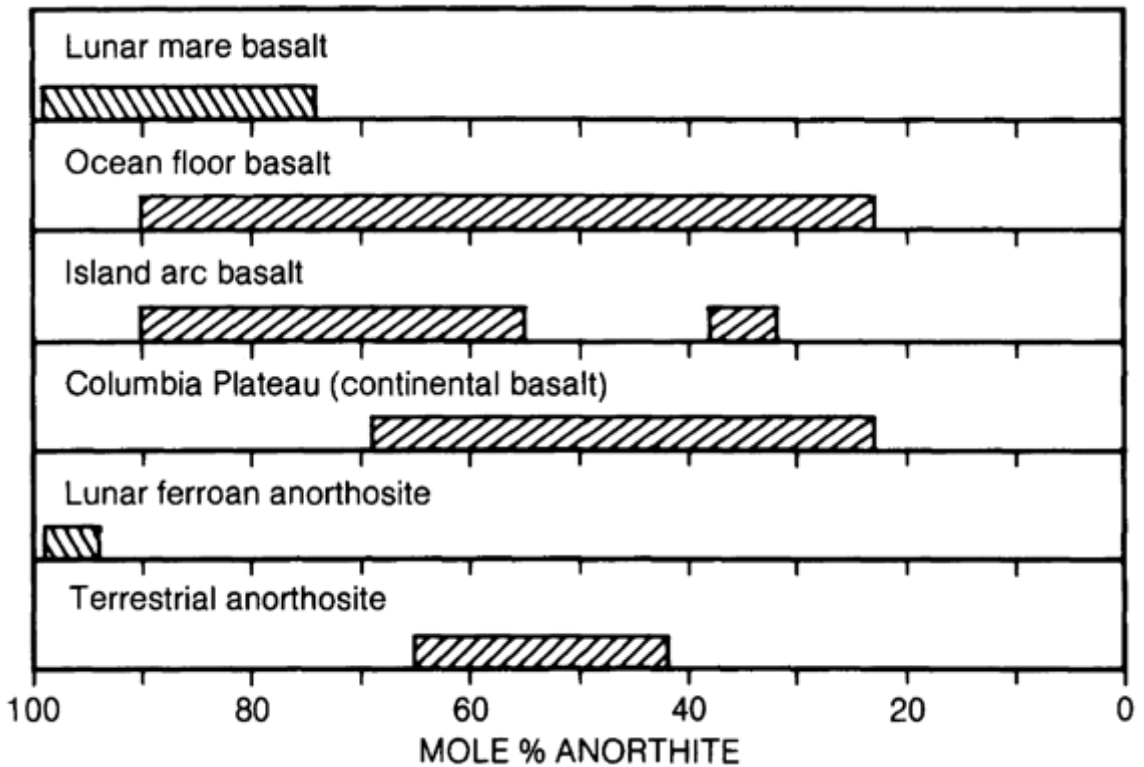


Figure 31. Comparison of anorthite composition in terrestrial and lunar rocks (Papike, Taylor and Simon, 1991).

The samples were sent for characterization with a Rigaku SmartLab X-ray Diffractometer (XRD) at Surface Science Western. XRD works based on Bragg's Law as shown in Figure 32, where two parallel X-rays with a wavelength of λ were reflected from two mineral crystal lattices at an angle of θ . The lattices have a distance of d in between, which will be calculated when X-ray is sent back to the receiver using the following equation (Le Pevelen, 2010):

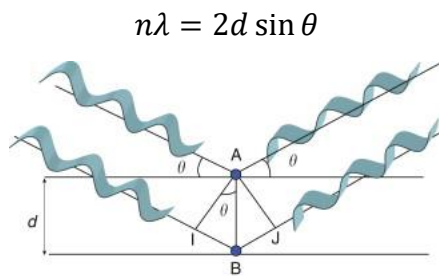


Figure 32. Bragg's law in XRD (Le Pevelen, 2010).

To prepare each sample for characterization, a small quantity of each simulant was further ground with an agate mortar and pestle for at least 20 minutes until powdery, as seen in Figure 33. Samples were characterized between 5 to 90 degrees, with 0.02 degrees per step and 3 degrees per minute. The XRD source for this machine is copper, and a Ni-KB filter was applied during characterization. The results were processed using the DIFFRAC.EVA Suite to match potential mineral phases within the samples.



Figure 33. Sample grinding in preparation of XRD characterization. Sample shown in the figure is the Mistastin impact melt used to produce UWO-1S.

2.5 Specific Gravity

The Specific Gravity (G_s), also called Specific Density or Specific Weight, refers to the ratio of a soil particle to water of the same volume at 4 °C (Carrier, Olhoeft and Mendell, 1991). Measurement of Apollo samples, including individual rock fragments yielded a range of specific gravities from 2.3 to higher than 3.2, of which a value of 3.1 is recommended for general scientific and engineering studies (Carrier, Olhoeft and Mendell, 1991). Testing specific gravity of a soil sample often requires to submerge the sample into a liquid or gas, such as distilled water, nitrogen or helium (Carrier, Olhoeft and Mendell, 1991). Chemical and mineralogical composition, and even weathering history could affect the specific gravity of terrestrial soils (Roy and Kumar Bhalla, 2017), but the shape of lunar regolith grains, such as the sub-granular voids within agglutinates where water (or other agents) cannot fill, could also impact the specific gravity of lunar regolith (Carrier, Olhoeft and Mendell, 1991).

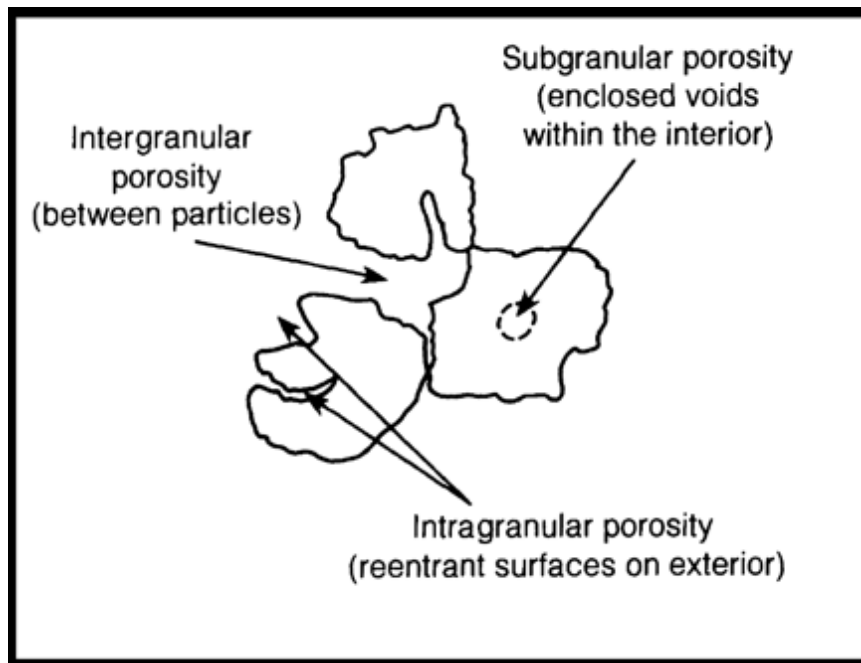


Figure 34. Example of different possible porosities within a lunar agglutinate (Carrier, Olhoeft and Mendell, 1991).

In terrestrial civil engineering, materials with higher specific gravity are preferred for constructing roads and foundations. It is also an important value used to calculate a few

other parameters, such as void ratio and porosity. Higher specific gravity might also result in higher shear strength (Roy and Kumar Bhalla, 2017).

The characterization of specific gravity followed the ASTM D854 standard. A clean, pre-weighed volumetric flask was first filled with 500ml of distilled water and connected to a vacuum source to remove excessive gas. After weighing again (water and flask), the flask was emptied and added with 100g of sample and filled to about 2/3 of the volume with distilled water and stirred. The temperature of the mixture was measured and then connected to a vacuum source again and de-aired for about 24 hours (Figure 35).



Figure 35. (Left) De-airing 500ml distilled water in a volumetric flask; (Right) De-airing sample mixture (LHS-1 pictured) for 24h.

When de-airing is complete, the flask was added with more distilled water to the 500ml mark and weighed. The specific gravity of each simulant was calculated using the following formulas:

$$G_s = \frac{M_s}{M_w} = \frac{M_s}{(M_1 + M_s) - M_2}$$

Where M_1 is the initial weight of flask with distilled water, M_2 is the weight of the flask with sample and de-aired water, M_s is the weight of the simulant sample added to the flask, and M_w is the weight of distilled water added to the flask after de-airing.

2.6 Density, Void Ratio

Lunar regolith is naturally very dense, with the relative density reaching up to 90% at just 30 cm below the lunar surface. Together with high cohesion, excavating and drilling the lunar surface is expected to be very challenging below just 30 cm even though the irregular particle shapes create a higher porosity (Just et al., 2020). In order to develop excavation technology for ISRU, higher fidelity of density, porosity, cohesion and angle of friction are usually required.

In this study, we aim to first determine the maximum and minimum densities and void ratios using a modified version of Proctor Compaction Method with a small acrylic cylindrical mould. To determine the minimum density and maximum void ratio, the sample was loosely poured into the pre-weighed mould through a funnel and carefully flattened on the top (Figure 36), then weighed for its mass with the mould as m_{loose} . Its minimum density and maximum void ratio could be then determined using the following equations:

$$V = \pi r^2 h$$

$$m_1 = m_{loose} - m_{mould}$$

$$D_{min} = m_1 \div V$$

$$e_{max} = (G_s \div D_{min}) - 1$$

Where V , r and h are the volume, radius and height of the mould.



Figure 36. Sample (LHS-1 pictured) is loosely sprinkled into the mould through a funnel (left) and flattened with a spatula at the top (right).

To obtain the maximum density, the mould was emptied and re-filled to about half its depth. A weight was added to the top to maintain the sample quantity, and the system was placed on a vibrating platform for five minutes (Figure 37). During vibration, the grains would rearrange their positions and naturally compact to the tightest possible state. This step was repeated until the mould is filled to the top and flattened, and a new sample mass m_2 is determined by weighing the mould with the compact sample, then subtract the weight of the mould. The maximum density D_{max} and minimum void ratio e_{min} were determined using the same equations.



Figure 37. Sample (LHS-1 pictured) was added to half the mould's depth (left) and vibrated for natural compaction with a weight to stop any loss in quantity (right). This step was repeated until the mould was fully filled with compacted sample.

2.7 Consolidation

During terrestrial construction, consolidation (compression) of soil could be caused by re-packing of grains, seeping water, particle deformation and elastic distortions (Roy and Kumar Bhalla, 2017). While the lunar environment (e.g. low gravity, lack of water) might not affect construction in similar manner, and that different constructional approaches might avoid these known concerns, it could still help to evaluate how compressibility within simulants could affect the decision of designing lunar infrastructure.

The consolidation properties of the simulants used for this study were tested with a VJ Tech ACONS II oedometer. During characterization, the samples were pressed within a ring container under pre-defined pressure stages and measured for the depth changed at each pressure value. For this study, all samples were compressed from 30% relative density.

The amount of sample used for each test should be determined in advance using the following formulas:

$$D_r = \frac{e_{max} - e}{e_{max} - e_{min}}$$

$$e = \frac{G_s \times \gamma_w}{D_{dry}} - 1$$

$$m_{sample} = D_{dry} \times V$$

Where D_r was the relatively density aimed for this characterization at 30%, γ_w is the unit weight of water, which is always 1, and V is the volume of the ring container. e_{max} , e_{min} and G_s of the sample were determined from the Proctor Test.

To set up each characterization, the sample was loosely sprinkled into the ring container, then gently pressed to flatten the top without losing any mass or create surface depression. After leveling the top surface, it was placed into a cylindrical container and loaded into the oedometer as shown in Figure 38.

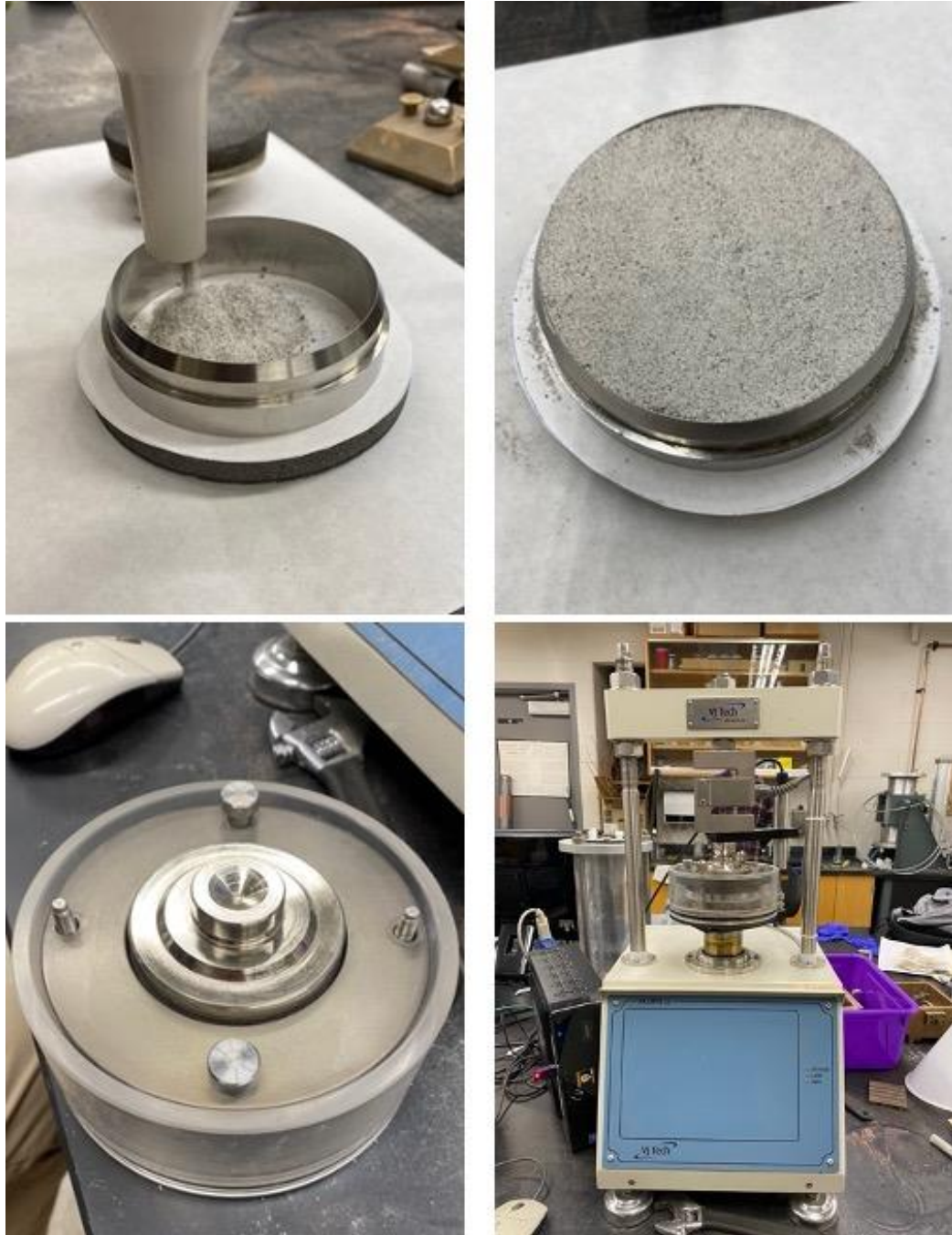


Figure 38. Sample (LHS-1 pictured) was loosely sprinkled into the ring mould (upper left) and carefully flattened (upper right). After levelling, the mould was placed into a cylindrical container (lower left) and loaded into the oedometer for consolidation (lower right).

The tests were performed using the csOedo software, where each sample was set to be compressed at 5kPa (sitting load, not used for calculation), 10kPa, 20kPa, 40kPa, 80kPa, 160kPa, 320kPa, and 640kPa. When reaching the highest load setting, the equipment will gradually loosen the pressure back to 10kPa using the same load settings in the reverse order. Each load was settled for one hour before moving on to the next load.

Chapter 3

3 Results

This chapter displays the results of the simulants as characterized by the methods described in Chapter 2, with some comments explaining the findings and possible implications.

3.1 Mineralogy

Figure 39 shows the XRD patterns with matched minerals. As simulants were highland type, the results showed strong indication of plagioclase feldspar components.

As UWO-1G (Greenspar) is the major component for LHS-1, the results of these two simulants are almost identical. Following Gruener et al. (2020)'s result, high-An plagioclase such as bytownite and anorthite were confirmed being the predominant component for both, and LHS-1 showed additional signals for minor components such as olivine, pyroxene and ilmenite as indicated on the product datasheet.

The breccia used for UWO-1S also showed strong signal on the presence of plagioclase feldspar which is likely Na-rich anorthite. However, a slight curve on the original signal between 20 – 30° can also be seen, indicating the presence of glass in this feedstock. The melt rock, on the other hand, was more complex in composition, but the main component was also plagioclase, possibly a mixture of anorthite and labradorite.

Additionally, UWO-1G, UWO-1S breccia, and mixed UWO-1S are found with small amounts of quartz. While quartz is very rare on the Moon (Papike, Taylor and Simon, 1991), it is abundant on Earth and hard to avoid if processing natural resources when producing simulants. However, quartz could be potentially helpful when testing with material durability as it is an abrasive mineral.

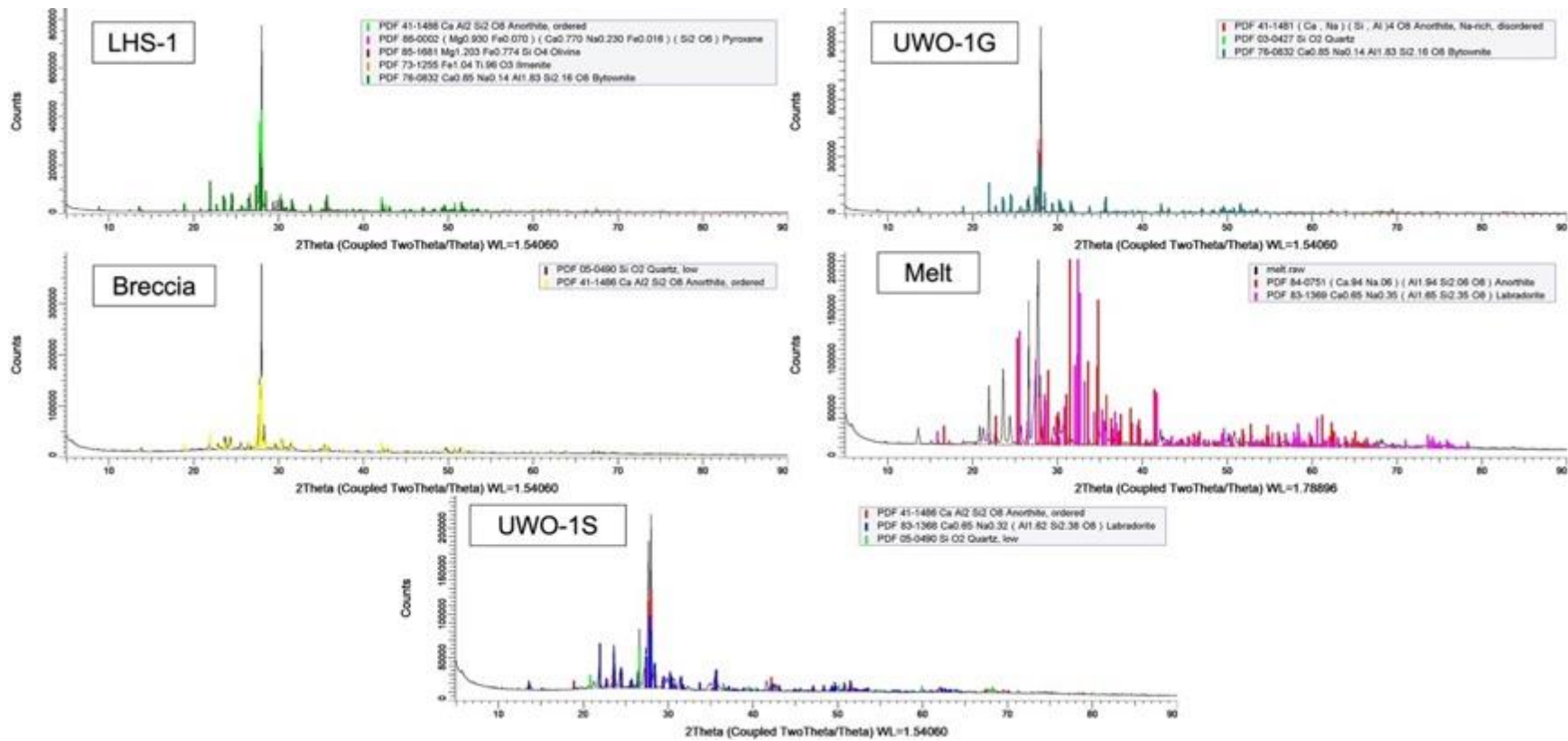


Figure 39. XRD patterns with matched mineral candidates. The backgrounds are kept for demonstrating a slight curve within the breccia and UWO-1S around the range of 20 - 30°, which indicates the presence of glass.

3.2 Particle Shape

SEM images of the simulant samples are compiled in Figure 40. LHS-1, UWO-1G and UWO-1S breccia all demonstrated some angularity and elongated shape, where UWO-1S melt appeared to be less angular and not many elongated grains despite containing anorthosite compositions like others. The broken surface of the UWO-1S components appear to be more irregular and not smooth compared to LHS-1 and UWO-1G.

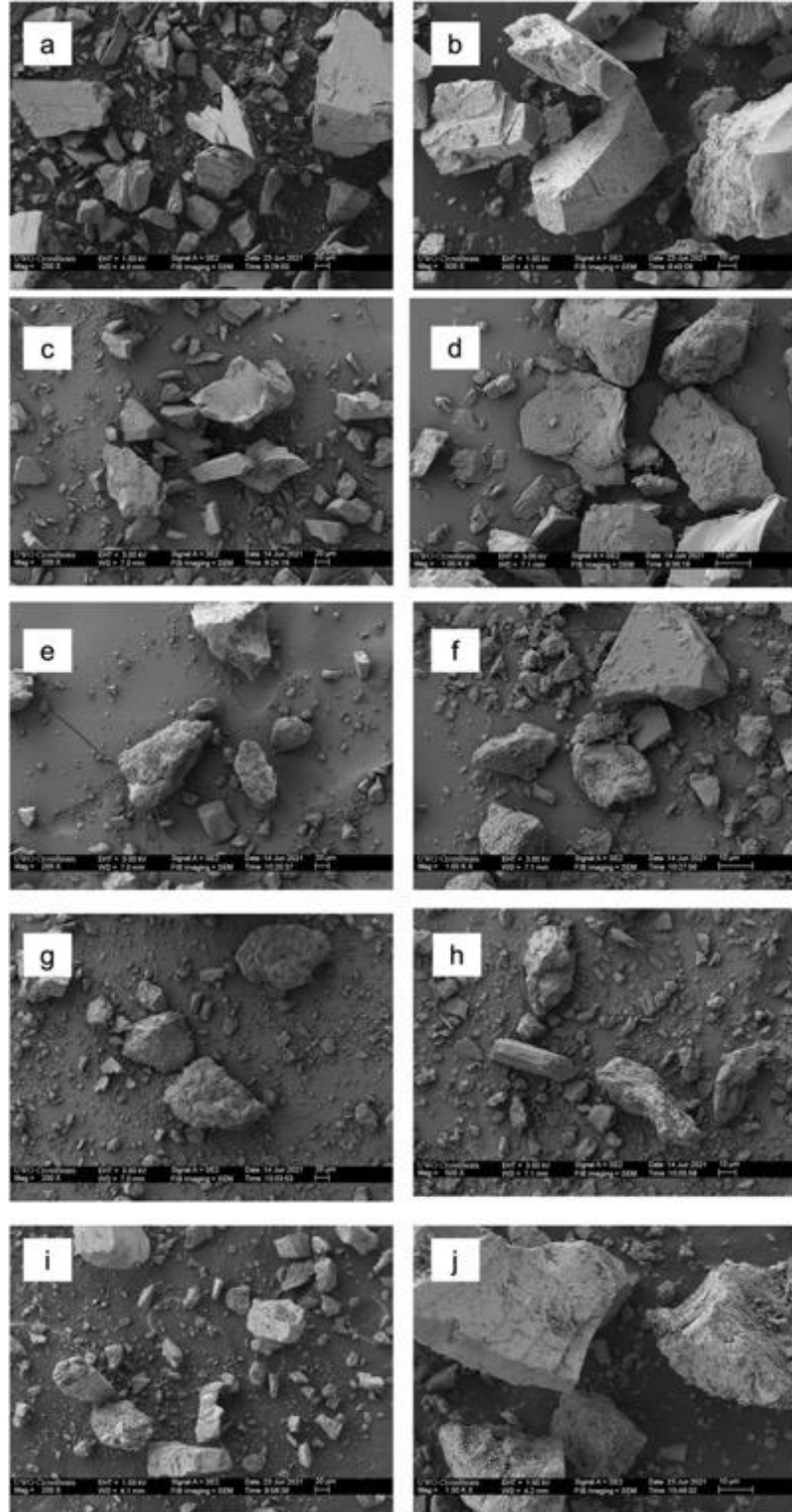


Figure 40. SEM images of LHS-1 (a,b), UWO-1G (c,d), UWO-1S breccia (e,f), UWO-1S melt (g,h), and UWO-1S mixed (i, j). Scale bars in the left column images are 20µm, and 10µm on the right column.

3.3 Particle size distribution

The particle sizes of the original simulants (including melt and breccia components of UWO-1S) simulants were closely matched to that of LHS-1. Figure 41 shows the results of sieve analysis of all five simulants/components, and Figure 42 shows the results of hydrometer analysis of the fines. The overall particle size distributions are presented in Figure 43.

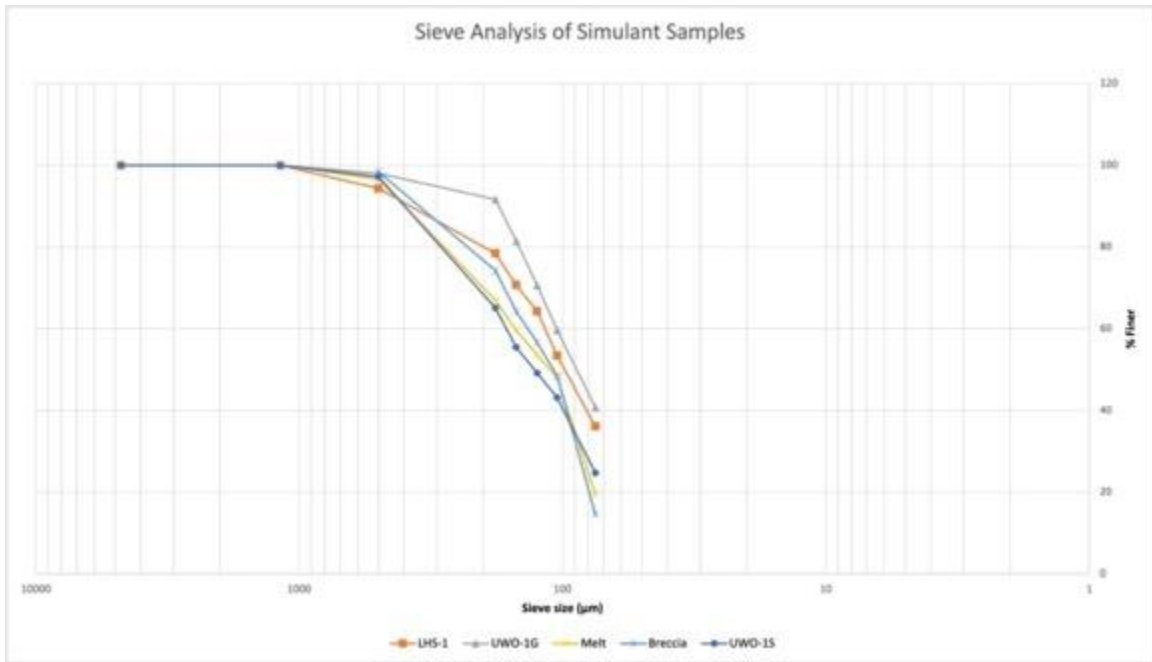


Figure 41. Sieve analysis of simulant samples used for this study.

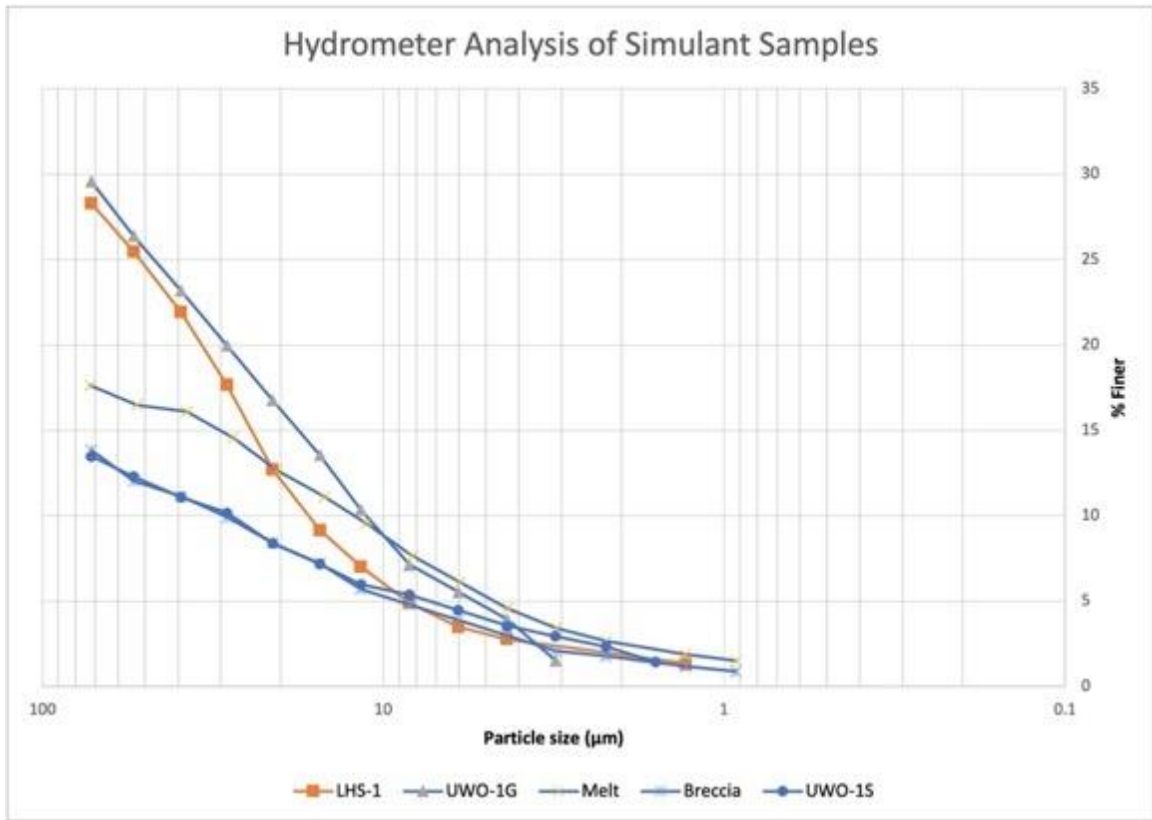


Figure 42. Hydrometer analysis of simulant samples used for this study.

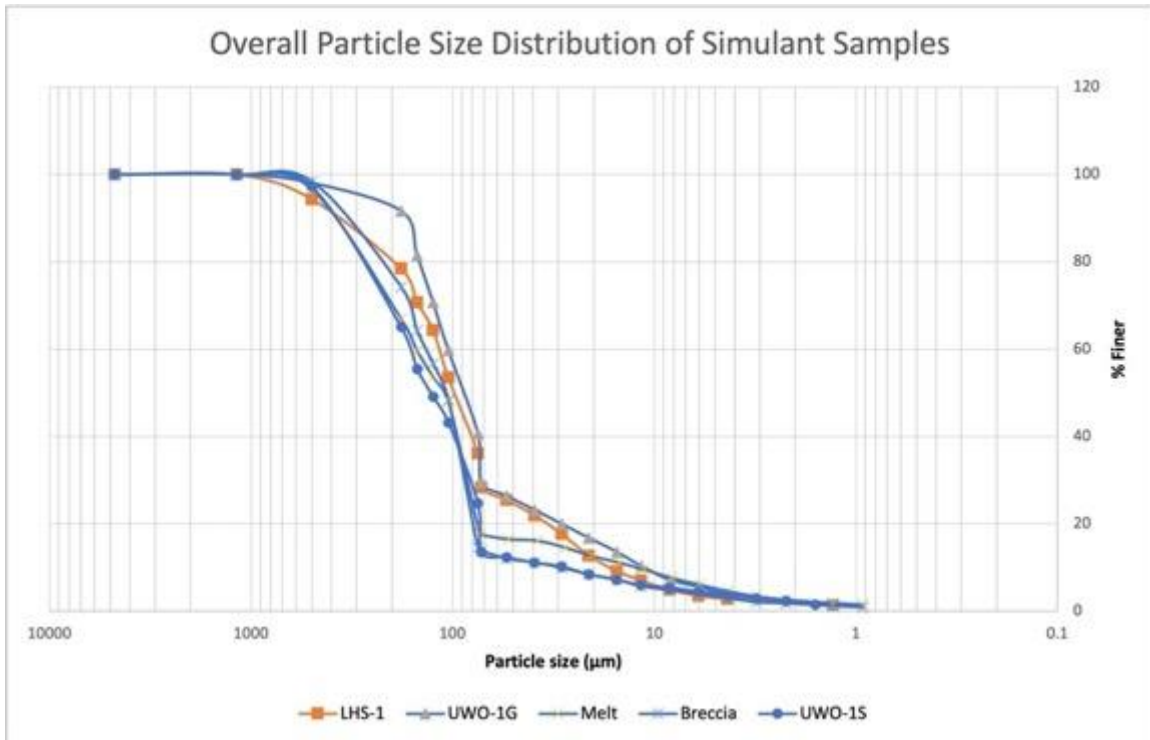


Figure 43. Overall Particle size distribution of the simulant samples used for this study, combined with both sieve and hydrometer analysis results.

3.4 Density, void ratio, and specific gravity

Table 11 summarizes the density and void ratios of the simulants determined from the Proctor Compaction Test, as well as their respective specific gravity. Corresponding reference values of real lunar regolith as discussed in Chapter 2, as well as two additional lunar highland simulant properties are also presented on the bottom rows for comparison. Due to an untimely equipment malfunction which could not be repaired at the time of completing characterizations, UWO-1S specific gravity was estimated to be the average of its two components, since the product was mixed on a 1:1 ratio.

LHS-1 and UWO-1G have higher specific gravity and density, where UWO-1S components and the final mix are relatively low, compared to the known ranges of lunar regolith. However, missing components such as agglutinates and np-Fe could have contributed to the differences as well.

Table 11. Maximum and minimum densities and void ratios, and specific gravity of each simulant. Information of lunar regolith was taken from Carrier, Olhoeft and Mendell, (1991), OPRH2N taken from Zhang, et al. (2019) and Newson et al. (2021).

Simulant	D_{min} (g/cm ³)	e_{max}	D_{max} (g/cm ³)	e_{min}	G_s
LHS-1	1.31	1.08	1.86	0.46	2.73
UWO-1G	1.30	1.09	1.89	0.44	2.72
UWO-1S (breccia)	1.06	1.36	1.67	0.51	2.51
UWO-1S (melt)	1.25	1.17	1.72	0.57	2.70
UWO-1S (mixed)	1.15	1.26**	1.77	0.47**	2.61*
Lunar regolith ***	1.50 ± 0.05	1.07 ± 0.07	1.74 ± 0.05	0.78 ± 0.07	2.3 – 3.2+
OPRH2N	1.37	1.12	1.84	0.57	2.90

*Estimation

** Calculated based on estimation

*** Lunar regolith values are average bulk density and void ratio at the top 15 cm from the lunar surface (D_{min} , e_{max}), and 30-60 cm below the lunar surface (D_{max} , e_{min})

3.5 Consolidation

Appendix G and Figure 44 shows the value and plotted trends of void ratio change during consolidation tests for all simulants. The UWO-1S individual components, which had higher void ratio values to begin with, were compressed more than the LHS-1 and UWO-

1G samples. The respective values for the maximum and minimum void ratio differences were 0.165 (LHS-1), 0.123 (UWO-1G) 0.278 (UWO-1S breccia) and 0.207 (UWO-1S melt).

The mixed UWO-1S result was not included at this time as some critical value is missing due to the aforementioned equipment malfunction, but it is likely that it will exhibit the same pattern as its individual components with poor ability to regain void ratio.

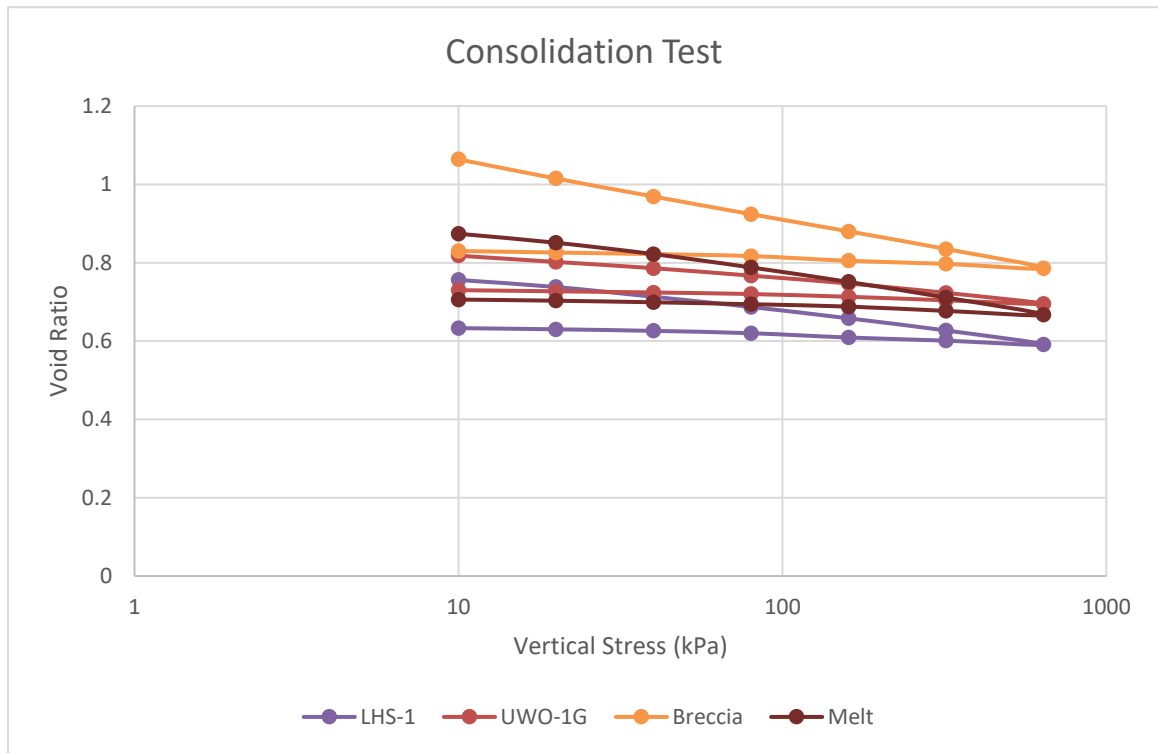


Figure 44. Consolidation results of simulants.

Chapter 4

4 Discussions

For this study, three types of lunar highland simulants were compared with some of their fundamental properties: LHS-1, a commercial product that has higher mineralogical fidelity; UWO-1G, an original product that used only Greenspar, the anorthosite feedstock that is also the major component of LHS-1; and UWO-1S, another original product, which was created from grinding impact rocks as an attempt to produce shocked grains in simulants for future research.

This chapter discusses the results obtained on all simulants based on their physical and mineralogical properties. As the characterizations performed for this study were limited, some potential future work will also be suggested for further analyses of the same simulants, as well as for improving the fidelity for future simulants.

4.1 Mineralogy

The compositions of all simulants were not complicated. XRD characterization showed consistency of high-An (Ca-rich) plagioclase minerals, such as anorthite, bytownite and labradorite to be the major components for all simulants. However, only the Mistastin breccia showed a slight indication of glass present in the feedstock, not in the melt rock or LHS-1/UWO-1G. Minor components listed in LHS-1's datasheet, such as ilmenite, olivine and pyroxene, were also confirmed through XRD.

Quartz was also found in most products. While it is difficult to avoid as it commonly exists on Earth but rare on the Moon, it could be of use in testing anti-abrasive materials in some cases.

4.2 Physical properties

UWO-1G and UWO-1S were created to closely match the particle size distribution with each other, as well as with LHS-1. The proximity, combined with the mineralogical characterization results, allowed the fair comparison of the other physical properties, such as density and void ratio, specific gravity, and compressibility (consolidation).

All simulants were less dense and have lower specific gravity values compared to those of typical lunar regolith, although they mostly fit within the known ranges of these physical properties. Out of all the simulants, the UWO-1S breccia component was the least dense and exhibited highest void ratio. When compressed with the oedometer, the breccia component also had the largest difference of void ratio compared to the beginning, meaning that its particles were easier to be compressed compared to the non-shocked simulants. The melt rock component, while has similar specific gravity and density values to LHS-1 and UWO-1G, its particle shapes were more rounded and exhibited highly irregular broken surfaces out of all samples, and demonstrated higher compressibility, although not as much as the breccia. A possible reason that caused such differences in their physical properties could be that the impact rocks, especially the breccia, were heavily fractured as seen in Figure 19. These fractures created some additional void spaces within the rock and subsequently, their ground grains. This is also a possible reason that the rock broke down along these irregular fractures and therefore displayed rougher surfaces.

One potential way to increase the specific gravity and density is through introducing additional components. For example, the OPRH2N simulant result characterized by Zhang et al., (2019) used to compare with this study is a mechanical simulant developed by Off Planet Research LLC., where they mixes up to 30% of basaltic content into the highland simulant. Another highland simulant example is OB-1, where olivine glass slag was mixed into the Archean Shawmere anorthosite feedstock (Battler, 2008), which happened to be the 70% component of OPRH2N as well (Zhang et al., 2019).

The Mistastin rocks used in this study were shocked with a pressure up to 60 GPa, but a study by Pernet-Fisher et al. (2017) suggested that lunar anorthosite generally went through weak shock levels <15 GPa, where higher shock level at over 30 GPa is uncommon. The lower gravitational force on the Moon could be a reason that affects the crater-forming conditions (Ivanov, 1976; Nolan et al., 1996), however, it is also possible that the study by Pernet-Fisher et al. is not completely representative of the entire lunar surface, since it was performed on selected Apollo highland samples and one meteorite. Such difference may lead to different mechanical behaviours than those of real lunar regolith. Comparison with

less shocked rocks, and with new lunar highland regolith samples, may be considered for further work.

4.3 Other considerations

In this study, none of the simulants contained additional components such as agglutinates, nanophase-iron, or solar wind-implanted elements, which is a common practice in most simulants. However, some of these components could alter test results as well. An example study carried out by Matsushima et al., (2010) with lunar agglutinate simulant under consolidation test suggested that they are much more likely to be compressed (i.e., particles will be crushed during compression and not able to regain void ratio).

The UWO-1S feedstocks were previously collected from the Mistastin Crater in Canada, which is one of the only two anorthositic impact structures known in the world (the other one is the Manicouagan Crater in Quebec, Canada, see Spray et al. (2010)). The limited option of locations will bring difficulties in logistics and transportation, should future investigations that require the same feedstocks are needed in other parts of the world.

4.4 Potential future work

With heavily restricted access to materials and facilities due to the COVID-19 pandemic, the quantities of simulants produced for this study were very low (less than 2 kg). Although enough to perform the characterizations included in this study, the results may have limited level of confidence. Should this work to be continued for other characterizations and better representative results, at least 10 -15 kg of each product are needed.

The characterizations performed in this study gave preliminary insight on the possibility of creating shocked grains within lunar simulants from pulverizing impact rocks. Even though the results are certainly not sufficient yet to give solid conclusions on whether the attempt was successful or not, the current results did indicate the likelihood that the UWO-1S simulant does have a weaker grain strength and deform easier than simulants produced from non-shocked feedstock. Some immediate follow-up characterizations, such as shear strength tests on the samples and examining their particle size distribution and particle shapes again, may be useful for the interpretation.

Similarly, although there were no significant findings about whether the composition differences between LHS-1 and UWO-1G have affected the properties characterized in this study, it does not mean that the mineralogical fidelity is not important in other cases. Evaluating more properties listed in **Appendix D** could provide more results to support the discussion.

Another potential comparison could be made with creating a lunar mare simulant from basaltic impact rocks. One of the potential sourcing locations could be the Lonar Crater located in India, which was proposed as a terrestrial analogue to study impact effects on basalts on other planetary bodies, since it is one of the rare impact structure that was entirely located on a volcanic basalt province (Kumar, 2005).

As this study produced only small amounts of UWO-1G and UWO-1S for preliminary characterization, a small-size pulverizer could satisfy the production requirement. However, if similar products are required in larger quantities, industrial equipment such as ball mills might be necessary, and the result of grinding could be compared with this study to determine if processing methods will affect the physical properties.

Chapter 5

5 Conclusions

Functional analogues are critical tools that allow us to explore space using materials found on Earth that have certain similarities to our study targets. Among the examples of analogue samples, planetary regolith simulants are one of the most well-known examples. Lunar regolith simulants can help with testing future lunar surface exploration equipment and investigate ISRU applications to ensure safer and long-duration missions.

As analogues are mostly never perfect replicas of extraterrestrial targets, each type of lunar simulants is also produced to simulate limited properties to serve specific test purposes. With the advancement of our understanding in lunar regolith and environment, the quality of simulants has been improved in the past few decades, such as the creation of agglutinated grains and glass spherules. However, there are still many properties not being simulated, and their importance are not widely discussed. On the other hand, there is a common issue within the simulant user community, which is the misuse of simulants outside its originally intended purposes.

This study was formed from two questions: 1) How mineralogical accuracy affects the behaviours of lunar simulants; and 2) If it is possible to produce shocked (e.g. fractured, lower strength) grains, which has rarely been attempted in the past and its importance is not well known. To address these two questions, three types of lunar highland simulants were compared with each other, of which two were created on-campus as original products.

LHS-1, as a commercial product available from Exolith Lab, was produced by mixing different components to approximate the average Apollo highland sample mineralogy. Its major component, the Greenland White Mountain anorthosite “Greenspar”, was provided by Hudson Resources Inc. and was used to create the original simulant UWO-1G without any additional components for comparison of fundamental properties.

UWO-1S was created as an attempt to create shocked grains in simulants. Previous attempts were mostly focused on artificially shock lunar simulants, which was difficult and

costly. UWO-1S reversed the order of production, by selecting anorthositic impact rocks, which are already shocked in nature, and pulverizing into fine grains.

Although mineralogical characterization suggested that all simulants contained high-An plagioclase mineral(s) as the main component, and the two original products were ground using the same pulverizer, SEM imaging revealed that the impact rock grounds tend to exhibit higher irregularity in particle shapes compared to the unshocked LHS-1 and UWO-1G, and their surface appear to be rougher as well.

Another difference noticed was that even though all simulants have similar particle size distributions, the UWO-1S components, especially the breccia, had a significantly lower specific gravity and higher void ratio. This may be caused by the impact event that formed the Mistastin crater had heavily fractured the rock as seen in their thin sections, and therefore created additional void spaces. These two feedstocks also showed higher compressibility during consolidation tests, which is a possible indication that the grain strength is weaker compared to non-shocked feedstocks.

Due to COVID-19 pandemic, the scope of this study was unfortunately limited, as well as the availability of resources and facilities to perform characterizations. Although it may not be sufficient to prove the success of creating shocked grains yet, the results obtained from this study so far indicated a high possibility. producing more quantities of these products and perform additional tests, such as the friction angle and cohesion, as well as follow-up characterizations on particle size distribution and particle shapes will be helpful to provide more values to make a confident conclusion. Similarly, the mineralogical accuracy between LHS-1 and UWO-1G did not show much impact on their behaviours at this stage, but further tests, especially related to ISRU, may provide new results.

Additionally, all three simulants only included mineral and rock grains, without additional components such as agglutinates, np-Fe or solar wind-deposited elements added. Including more components into the simulants could also potentially improved the test results, however financial and technological restrictions may limit the possibility of creating such components.

Proper production, utilization and storage of simulants often require significant efforts in interdisciplinary understanding and cooperation (e.g. natural and medical sciences, engineering, management), which is becoming more prominent with the growth of the simulant user community and excellent, innovative ideas. It is hopeful that this study will first contribute to the discussion of the importance on shocked grains and mineralogical fidelity in lunar simulants, especially when related to ISRU research topics, and act as an education source on understanding the differences of lunar regolith simulants.

References

- Allton, J.H., Galindo Jr., C. and Watts, L.A., 1985. Guide to Using Lunar Soil and Simulants for Experimentation. In: *Lunar bases and space activities of the 21st century (A86-30113 13-14)*. Houston: Lunar and Planetary Institute.pp.497–506.
- Ashwal, L.D. and Burke, K., 1987. Types and Characteristics of Terrestrial Anorthosites. In: *Lunar and Planetary Science Conference*. Lunar and Planetary Institute.pp.34–35.
- ASTM International, 2017. *Standard Test Method for Particle-Size Distribution (Gradation) of Fine-Grained Soils Using the Sedimentation (Hydrometer) Analysis*. ASTM International, .
- Bart, G.D., Nickerson, R.D., Lawder, M.T. and Melosh, H.J., 2011. Global survey of lunar regolith depths from LROC images. *Icarus*, [online] 215(2), pp.485–490. Available at: <<http://dx.doi.org/10.1016/j.icarus.2011.07.017>>.
- Battler, M., 2008. *Development of an anorthositic lunar regolith simulant: OB-1*. The University of New Brunswick.
- Battler, M.M. and Spray, J.G., 2009. The Shawmere anorthosite and OB-1 as lunar highland regolith simulants. *Planetary and Space Science*, [online] 57(14–15), pp.2128–2131. Available at: <<http://dx.doi.org/10.1016/j.pss.2009.09.003>>.
- Boslough, M.B., Bernold, L.E. and Horie, Y., 1992. Shock-treated lunar soil simulant: Preliminary Assessment as a Construction Material. In: R.C. Elphic and D.S. McKay, eds. *Lunar and Planetary Inst., Joint Workshop on New Technologies for Lunar Resource Assessment*. Santa Fe.pp.14–15.
- Cain, J.R., 2010. Lunar dust: The Hazard and Astronaut Exposure Risks. *Earth, Moon and Planets*, 107(1), pp.107–125.
- Cameron, A.G.W. and Ward, W.R., 1976. The origin of the Moon. pp.120–122.
- Cannon, K.M. and Britt, D.T., 2019. Mineralogically Accurate Simulants for Lunar

ISRU, and Strategic Regolith Processing. In: *Developing a New Space Economy 2019*. [online] Available at: <<http://sciences.ucf.edu/class/planetary-simulant->>.

Carrier, W.D., Olhoeft, G.R. and Mendell, W., 1991. Physical Properties of the Lunar Surface. In: G.H. Heiken, D.T. Vaniman and B.M. French, eds. *Lunar Sourcebook: A User's Guide to the Moon*. Cambridge University Press. pp.475–594.

Caston, R., Luc, K., Hendrix, D., Hurowitz, J.A. and Demple, B., 2018. Assessing Toxicity and Nuclear and Mitochondrial DNA Damage Caused by Exposure of Mammalian Cells to Lunar Regolith Simulants. *GeoHealth*, 2(4), pp.139–148.

Currie, K.L., 1968. Mistastin Lake, Labrador: A new Canadian crater. *Nature*, 220(5169), pp.776–777.

Currie, K.L., 1971. Geology of the resurgent cryptoexplosion crater at Mistastin Lake, Labrador. *Bulletin - Geological Survey of Canada*, [online] 207, p.62 p. Available at: <https://www.lib.uwo.ca/cgi-bin/ezpauthn.cgi?url=http://search.proquest.com/docview/52532643?accountid=15115%0Ahttp://sfx.scholarsportal.info/western?url_ver=Z39.88-2004&rft_val_fmt=info:ofi/fmt:kev:mtx:journal&genre=article&sid=ProQ:ProQ:georefmodule&atitle>.

Dawes, P.R., 2009. The bedrock geology under the Inland Ice: The next major challenge for Greenland mapping. *Geological Survey of Denmark and Greenland Bulletin*, (17), pp.57–60.

Elardo, S., 2016. Lunar Magma Ocean Theory, Origins, and Rationale. In: B. Cudnik, ed. *Encyclopedia of Lunar Science*. [online] Cham: Springer International Publishing. pp.1–8. Available at: <https://doi.org/10.1007/978-3-319-05546-6_25-1>.

Elkins-Tanton, L.T., Burgess, S. and Yin, Q.Z., 2011. The lunar magma ocean: Reconciling the solidification process with lunar petrology and geochronology. *Earth and Planetary Science Letters*, [online] 304(3–4), pp.326–336. Available at: <<http://dx.doi.org/10.1016/j.epsl.2011.02.004>>.

Engelschiøn, V., Cowley, A., Fateri, M., Coene, S., Siarov, S. and Cristoforetti, S., 2017. Human Exploration Initiatives at EAC: Spaceship EAC and the Development of Large-Volume Lunar Regolith Simulant for LUNA. In: *European Planetary Science Congress*. [online] Riga: EPSC. Available at:

<https://www.researchgate.net/publication/332343996_Human_Exploration_Initiatives_at_EAC_Spaceship_EAC_and_the_Development_of_Large-Volume_Lunar_Regolith_Simulant_for_LUNA>.

Exolith Lab, 2021. *LHS-1 Lunar Highlands Simulant*. [online] Available at:

<<https://exolithsimulants.com/collections/regolith-simulants/products/lhs-1-lunar-highlands-simulant>> [Accessed 3 Aug. 2021].

Exolith Lab, 2021. *LHS-1 Spec Sheet*. [online] University of Central Florida. Available at: <<https://cdn.shopify.com/s/files/1/0398/9268/0862/files/lhs-1-spec-sheet-2021.pdf?v=1611877987>> [Accessed 12 Jun. 2021].

Fa, W. and Jin, Y.Q., 2007. Quantitative estimation of helium-3 spatial distribution in the lunar regolith layer. *Icarus*, 190(1), pp.15–23.

Fa, W. and Jin, Y.Q., 2010. A primary analysis of microwave brightness temperature of lunar surface from Chang-E 1 multi-channel radiometer observation and inversion of regolith layer thickness. *Icarus*, [online] 207(2), pp.605–615. Available at: <<http://dx.doi.org/10.1016/j.icarus.2009.11.034>>.

Fa, W., Zhu, M.H., Liu, T. and Plescia, J.B., 2015. Regolith stratigraphy at the Chang'E-3 landing site as seen by lunar penetrating radar. *Geophysical Research Letters*, 42(23), pp.10179–10187.

Foucher, F., Hickman-Lewis, K., Hutzler, A., Joy, K.H., Folco, L., Bridges, J.C., Wozniakiewicz, P., Martínez-Frías, J., Debaille, V., Zolensky, M., Yano, H., Bost, N., Ferrière, L., Lee, M., Michalski, J., Schroeven-Deceuninck, H., Kminek, G., Viso, M., Russell, S., Smith, C., Zipfel, J. and Westall, F., 2021. Definition and use of functional analogues in planetary exploration. *Planetary and Space Science*, 197(September 2020).

- Geiss, J. and Rossi, A.P., 2013. *On the chronology of lunar origin and evolution: Implications for Earth, Mars and the Solar System as a whole. Astronomy and Astrophysics Review*, .
- Gråe Jørgensen, U., Appel, P.W.U., Hatsukawa, Y., Frei, R., Oshima, M., Toh, Y. and Kimura, A., 2009. The Earth-Moon system during the late heavy bombardment period - Geochemical support for impacts dominated by comets. *Icarus*, [online] 204(2), pp.368–380. Available at: <<http://dx.doi.org/10.1016/j.icarus.2009.07.015>>.
- Grieve, R.A.F., 1975. Petrology and chemistry of the impact melt at Mistastin Lake crater, Labrador. *Bulletin of the Geological Society of America*, 86(12), pp.1617–1629.
- Gruener, J.E., Deitrick, S.R., Tu, V.M., Clark, J. V., Ming, D.W. and J., C., 2020. Greenland ‘White Mountain’ Anorthosite: A New Lunar Polar Regolith Simulant Component. In: *51st Lunar and Planetary Science Conference*. Houston.pp.1–2.
- Guo, L., Wang, P., Zhu, S., Zuo, G., Peng, K., Wang, Q., Guo, B., Li, Z., Hou, Y., Zhang, D., Tian, L., Liang, L., Zhang, Z., Li, C., Chen, C. and Rao, J., 2013. *Crewed Lunar Base Project*. 1st ed. Beijing: China Astronautics Publishing House.
- Haldar, S.K., 2020. *Basic mineralogy. Introduction to Mineralogy and Petrology*.
- Hartmann, W.K. and Davis, D.R., 1975. Satellite-sized planetesimals and lunar origin. *Icarus*, 24(4), pp.504–515.
- Head, J.W. and Wilson, L., 1992. Lunar mare volcanism: Stratigraphy, eruption conditions, and the evolution of secondary crusts. *Geochimica et Cosmochimica Acta*, 56(6), pp.2155–2175.
- Hiesinger, H. and Head, J.W., 2006. New views of lunar geoscience: An introduction and overview. *Reviews in Mineralogy and Geochemistry*, 60, pp.1–81.
- Hill, P.J.A., Osinski, G.R. and Banerjee, N.R., 2020. Through the impact glass: Insight into the evolution of melt at the Mistastin Lake impact structure. *Meteoritics and Planetary Science*, 55(3), pp.591–621.

- Hörz, F., Grieve, R., Heiken, G., Spudis, P. and Binder, A., 1991. Lunar surface processes. In: *Lunar Sourcebook: A User's Guide to the Moon*. [online] pp.61–120. Available at:
<<https://pdfs.semanticscholar.org/aeef/1404b9cfd5a7d64e131894798cc2f4d2f8be.pdf>>.
- Ivanov, B.A., 1976. The effect of gravity on crater formation: thickness of ejecta and concentric basins. In: *7th Lunar Sci. Conf.* Lunar and Planetary Institute.pp.2947–2965.
- Jakus, A.E., Koube, K.D., Geisendorfer, N.R. and Shah, R.N., 2017. Robust and Elastic Lunar and Martian Structures from 3D-Printed Regolith Inks. *Scientific Reports*, 7, pp.1–8.
- Jamanca-Lino, G., 2021. Space Resources Engineering: Ilmenite Deposits for Oxygen Production on the Moon. *American Journal of Mining and Metallurgy*, 6(1), pp.6–11.
- Jia, Y., Shen, Z., Dang, Z., Wang, Q. and Tao, Z., 2014. Lunar soil simulant and its engineering application in lunar exploration program. *Spacecraft Environment Engineering*, 31(3), pp.241–247.
- Just, G.H., Smith, K., Joy, K.H. and Roy, M.J., 2020. Parametric review of existing regolith excavation techniques for lunar In Situ Resource Utilisation (ISRU) and recommendations for future excavation experiments. *Planetary and Space Science*, [online] 180(September 2019), p.104746. Available at:
<<https://doi.org/10.1016/j.pss.2019.104746>>.
- van Kan, M., 2011. *Physical and chemical properties of lunar magma*. Vrije Universiteit Amsterdam.
- Kanamori, H., Udagawa, S., Yoshida, T., Matsumoto, S. and Takagi, K., 1998. Properties of Lunar Soil Simulants Manufactured in Japan. New Mexico: Sixth ASCE Specialty Conference and Exposition on Engineering, Construction, and Operations in Space.
- Kaur, A. and Fanourakis, G.C., 2016. Effect of hydrometer type on particle size distribution of fine grained soil. *Proceedings of the 1st Southern African Geotechnical Conference, 2016*, pp.307–316.

- De Kestelier, X., Dini, E., Cesaretti, G., Colla, V. and Pambaguian, L., 2015. *Lunar Outpost Design*.
- Korotey, R.L., 2021. *Lunar Regolith Breccias and Fragmental Breccias*. [online] Available at: <<https://sites.wustl.edu/meteoritesite/items/lunar-regolith-breccias-and-fragmental-breccias/>> [Accessed 21 Jul. 2021].
- Kumar, P.S., 2005. Structural effects of meteorite impact on basalt: Evidence from Lonar crater, India. *Journal of Geophysical Research: Solid Earth*, 110(12), pp.1–10.
- Lai, J., Xu, Y., Zhang, X., Xiao, L., Yan, Q., Meng, X., Zhou, B., Dong, Z. and Zhao, D., 2019. Comparison of Dielectric Properties and Structure of Lunar Regolith at Chang'e-3 and Chang'e-4 Landing Sites Revealed by Ground-Penetrating Radar. *Geophysical Research Letters*, 46(22), pp.12783–12793.
- Landsman, Z., 2020. *Exolith Simulants Constituents Report*.
- LEAG and CAPTEM, 2010. *Status of Lunar Regolith Simulants and Demand for Apollo Lunar Samples*.
- Li, C., Su, Y., Pettinelli, E., Xing, S., Ding, C., Liu, J., Ren, X., Lauro, S.E., Soldovieri, F., Zeng, X., Gao, X., Chen, W., Dai, S., Liu, D., Zhang, G., Zuo, W., Wen, W., Zhang, Z., Zhang, X. and Zhang, H., 2020. The Moon's farside shallow subsurface structure unveiled by Chang'E-4 Lunar Penetrating Radar. *Science Advances*, 6(9), pp.1–9.
- Li, S., Lucey, P.G., Milliken, R.E., Hayne, P.O., Fisher, E., Williams, J.P., Hurley, D.M. and Elphic, R.C., 2018. Direct evidence of surface exposed water ice in the lunar polar regions. *Proceedings of the National Academy of Sciences of the United States of America*, 115(36), pp.8907–8912.
- Li, Y., Liu, J. and Yue, Z., 2009. NAO-1: Lunar Highland Soil Simulant Developed in China. *Journal of Aerospace Engineering*, 22(1), pp.53–57.
- Linke, S., Windisch, L., Kueter, N., Wanvik, J.E., Voss, A., Stoll, E., Schilde, C. and Kwade, A., 2020. TUBS-M and TUBS-T based modular Regolith Simulant System for

the support of lunar ISRU activities. *Planetary and Space Science*, [online] 180(March 2019), p.104747. Available at: <<https://doi.org/10.1016/j.pss.2019.104747>>.

Liu, Y., Park, J., Hill, E., Kihm, K.D. and Taylor, L.A., 2006. Morphology and physical characteristics of Apollo 17 dust particles. *Earth and Space 2006 - Proceedings of the 10th Biennial International Conference on Engineering, Construction, and Operations in Challenging Environments*, 2006(865), p.38.

Lucey, P.G., Neumann, G.A., Riner, M.A., Mazarico, E., Smith, D.E., Zuber, M.T., Paige, D.A., Bussey, D.B., Cahill, J.T., McGovern, A., Isaacson, P., Corley, L.M., Torrence, M.H., Melosh, H.J., Head, J.W. and Song, E., 2014. The global albedo of the Moon at 1064 nm from LOLA. *Journal of Geophysical Research: Planets*, 119, pp.1665-1679.

Luchsinger, K.M., Chanover, N.J. and Strycker, P.D., 2021. Water within a permanently shadowed lunar crater: Further LCROSS modeling and analysis. *Icarus*, 354.

Mader, M.M. and Osinski, G.R., 2018. Impactites of the Mistastin Lake impact structure: Insights into impact ejecta emplacement. *Meteoritics and Planetary Science*, 53(12), pp.2492–2518.

Mak, E., York, D., Grieve, R.A.F. and Dence, M.R., 1976. The age of the Mistastin Lake crater, Labrador, Canada. *Earth and Planetary Science Letters*, 31, pp.345–357.

Marion, C.L. and Sylvester, P.J., 2010. Composition and heterogeneity of anorthositic impact melt at Mistastin Lake crater, Labrador. *Planetary and Space Science*, [online] 58(4), pp.552–573. Available at: <<http://dx.doi.org/10.1016/j.pss.2009.09.018>>.

Matsushima, T., Katagiri, J., Ueda, T., Saiki, K., Tsuchiyama, A. and Ohtake, M., 2010. Particle properties and bulk mechanical properties of lunar surface soil. *Journal of the Japanese Society for Planetary Sciences*, 19(2), pp.105–111.

McKay, D.S. and Blacic, J.D., 1991. *Workshop on production and uses of simulated lunar materials: LPI Technical Report Number 91-01. Lunar and Planetary Institute. Houston.*

- McKay, D.S., Carter, J.L., Boles, W.W., Allen, C.C. and Allton, H.H., 1994. JSC-1: A New lunar soil simulant. In: *Proceedings of the 4th International Conference on Engineering, Construction and Operations in Space*. pp.857–866.
- McKay, D.S., Heiken, G., Basu, A., Blanford, G., Simon, S., Reedy, R., French, B.M. and Papike, J., 1991. The Lunar Regolith. In: G.H. Heiken, D.T. Vaniman and B.M. French, eds. *Lunar Sourcebook: A User's Guide to the Moon*. Cambridge University Press.
- Meurisse, A., Makaya, A., Willsch, C. and Sperl, M., 2018. Solar 3D printing of lunar regolith. *Acta Astronautica*, [online] 152(June), pp.800–810. Available at: <<https://doi.org/10.1016/j.actaastro.2018.06.063>>.
- Mitchell, J.K., Carrier, W.D., Houston, W.N., Scott, R.F., Bromwell, L.G., Durgunoglu, H.T., Hovland, H.J., Treadwell, D.D. and Costes, N.C., 1972. Soil mechanics. In: *Apollo 16 Preliminary Science Report*. Washington D. C.: NASA.
- Morris, R. V., 1976. Surface explore indices of lunar soils: A comparative FMR study. In: *7th Lunar Sci. Conf.* Lunar and Planetary Institute.pp.315–335.
- Morris, R. V., 1978. The surface exposure /maturity/ of lunar soils - Some concepts and Is/FeO compilation. In: *9th Lunar and Planetary Science Conference*. Lunar and Planetary Institute.pp.2287–2297.
- Nakamura, Y., Dorman, J., Duennebier, F., Lammlein, D. and Latham, G., 1975. Shallow lunar structure determined from the passive seismic experiment. *The Moon*, 13(1–3), pp.57–66.
- NASA, 2019. *Sls-Spec-159: Cross-Program Design Specification for Natural Environments*. [online] *NASA Technical Report Server*, Available at: <<https://ntrs.nasa.gov/citations/20200000867>>.
- NASA Earth Observatory, 2017. *Violent Formation for Mistastin Lake*.
- NASA History Office, 2007. *Apollo 11 Image Gallery*. [online] Available at:

<<https://history.nasa.gov/ap11ann/kippsphotos/apollo.html>> [Accessed 17 Feb. 2021].

Neuendorf, K.K.E., Mehl Jr., J.P. and Jackson, J.A., 2005. *Glossary of Geology*. 5th Editio ed. Alexandria: United Book Press.

Newson, T., Ahmed, A., Joshi, D., Zhang, X. and Osinski, G.R., 2021. Assessment of the Geomechanical Properties of Lunar Simulant Soils. In: *Earth and Space 2021*. Virtual Conference: ASCE.pp.146–156.

Noble, S., 2009. The Lunar Regolith. In: *Lunor Regolith Simulant Workshop*. Alabama: NASA.

Nolan, M.C., Asphaug, E., Melosh, H.J. and Greenberg, R., 1996. Impact craters on asteroids: Does gravity or strength control their size? *Icarus*, 124(2), pp.359–371.

O’Hara, K.D., 2018. Geology and Evolution of the Moon. In: *A Brief History of Geology*. Cambridge: Cambridge University Press.pp.211–233.

Oberbeck, V.R. and Quaide, W.L., 1968. Genetic implications of Lunar regolith thickness variations. *Icarus*, 9(1–3), pp.446–465.

Oberbeck, V.R., Quaide, W.L., Mahan, M. and Paulson, J., 1973. Monte Carlo calculations of lunar Regolith thickness distributions. *Icarus*, 19(1), pp.87–107.

Ouyang, Z., 2005. *Introduction to Lunar Science*. 1st Editio ed. Beijing: China Aerospace Publishing House.

Papike, J., Taylor, L. and Simon, S., 1991. Lunar minerals. In: G.H. Heiken, D.T. Vaniman and B.M. French, eds. *Lunar Sourcebook: A User’s Guide to the Moon*. Cambridge University Press.pp.121–181.

Pernet-Fisher, J.F., Joy, K.H., Martin, D.J.P. and Hanna, K.L.D., 2017. Assessing the shock state of the lunar highlands: Implications for the petrogenesis and chronology of crustal anorthosites. *Scientific Reports*, [online] 7(1), pp.1–12. Available at: <<http://dx.doi.org/10.1038/s41598-017-06134-x>>.

Le Pevelen, D.D., 2010. Small Molecule X-Ray Crystallography, Theory and Workflow. In: J.C. Lindon, G.E. Tranter and D.W. Koppenaal, eds. *Encyclopedia of Spectroscopy and Spectrometry*, 2nd ed. Elsevier.pp.2559–2576.

Pickersgill, A.E., Osinski, G.R. and Flemming, R.L., 2015. Shock effects in plagioclase feldspar from the Mistastin Lake impact structure, Canada. *Meteoritics and Planetary Science*, 50(9), pp.1546–1561.

Qian, Y., Xiao, L., Wang, Q., Head, J.W., Yang, R., Kang, Y., van der Bogert, C.H., Hiesinger, H., Lai, X., Wang, G., Pang, Y., Zhang, N., Yuan, Y., He, Q., Huang, J., Zhao, J., Wang, J. and Zhao, S., 2021. China's Chang'e-5 landing site: Geology, stratigraphy, and provenance of materials. *Earth and Planetary Science Letters*, 561.

Rai, R.K., Singh, V.P. and Upadhyay, A., 2017. Soil Analysis. In: R.K. Rai, V.P. Singh and A. Upadhyay, eds. *Planning and Evaluation of Irrigation Projects*. [online] Academic Press.pp.505-523. Available at: <<https://www.sciencedirect.com/science/article/pii/B9780128117484000170>>.

Rickman, D., Immer, C., Metzger, P., Dixon, E., Pendleton, M. and Edmunson, J., 2012. Particle shape in simulants of the lunar regolith. *Journal of Sedimentary Research*, 82(11), pp.823–832.

Roy, S. and Kumar Bhalla, S., 2017. Role of Geotechnical Properties of Soil on Civil Engineering Structures. *Resources and Environment*, [online] 7(4), pp.103–109. Available at: <<http://article.sapub.org/10.5923.j.re.20170704.03.html#Ref>>.

Ryder, G., 1981. *Distribution of rocks at the Apollo 16 Site. Workshop on Apollo 16, LPI Technical Report 81-01*. Houston: Lunar and Planetary Institute.

Ryu, B.-H., Wang, C.-C. and Chang, I., 2018. Development and Geotechnical Engineering Properties of KLS-1 Lunar Simulant. *Journal of Aerospace Engineering*, 31(1), p.04017083.

Sadrekarimi, A. and Olson, S.M., 2008. the Importance of Mineralogy and Grain Compressibility in Understanding Field Behavior of Failures. *6th International*

Conference on Case Histories in Geotechnical Engineering, (2), pp.1–9.

Sargeant, H.M., Abernethy, F.A.J., Barber, S.J., Wright, I.P., Anand, M., Sheridan, S. and Morse, A., 2020. Hydrogen reduction of ilmenite: Towards an in situ resource utilization demonstration on the surface of the Moon. *Planetary and Space Science*, [online] 180(September 2019), p.104751. Available at: <<https://doi.org/10.1016/j.pss.2019.104751>>.

Shukla, S., Tolpekin, V., Kumar, S. and Stein, A., 2020. Investigating the retention of solar wind implanted helium-3 on the moon from the analysis of multi-wavelength remote sensing data. *Remote Sensing*, 12(20), pp.1–24.

Sibille, L., Carpenter, P., Schlagheck, R. and French, R., 2006. *Lunar Regolith Simulant Materials: Recommendations for Standardization, Production, and Usage*. [online] NASA Technical Paper. Huntsville. Available at: <<https://ntrs.nasa.gov/archive/nasa/casi.ntrs.nasa.gov/20060051776.pdf>>.

Simon, S.B. and Papike, J.J., 1981. *The Lunar Regolith: Comparative Petrology of the Apollo and Luna SOils*. Lunar and Planetary Institute.

Song, H., Zhang, J., Sun, Y., Li, Y., Zhang, X., Ma, D. and Kou, J., 2021. Theoretical study on thermal release of helium-3 in lunar ilmenite. *Minerals*, 11(3), pp.1–14.

Spray, J.G., Thompson, L.M., Biren, M.B. and O'Connell-Cooper, C., 2010. The Manicouagan impact structure as a terrestrial analogue site for lunar and martian planetary science. *Planetary and Space Science*, [online] 58(4), pp.538–551. Available at: <<http://dx.doi.org/10.1016/j.pss.2009.09.010>>.

Spudis, P.D., Bussey, D.B.J., Butler, B., Carter, L., Chakraborty, M., Gillis-Davis, J., Goswami, J., Heggy, E., Kirk, R., Neish, C., Nozette, S., Patterson, W., Robinson, M., Raney, R.K., Thompson, T., Thomson, B.J. and Ustinov, E., 2010. RESULTS OF THE MINI-SAR IMAGING RADAR, CHANDRAYAAN-1 MISSION TO THE MOON. In: *41st Lunar and Planetary Science Conference*. Houston: Lunar and Planetary Institute. pp.1–2.

Sridharan, R., Ahmed, S.M., Pratim Das, T., Sreelatha, P., Pradeepkumar, P., Naik, N. and Supriya, G., 2010. 'Direct' evidence for water (H₂O) in the sunlit lunar ambience from CHACE on MIP of Chandrayaan I. *Planetary and Space Science*, [online] 58(6), pp.947–950. Available at: <<http://dx.doi.org/10.1016/j.pss.2010.02.013>>.

Taylor, L.A. and Meek, T.T., 2004. Microwave processing of lunar soil. *Science and Technology Series*, 108, pp.109–123.

Taylor, L.A. and Meek, T.T., 2005. Microwave Sintering of Lunar Soil: Properties, Theory, and Practice. *Journal of Aerospace Engineering*, 18(3), pp.188–196.

Vaniman, D., Reedy, R., Heiken, G., Olhoeft, G.R. and Mendell, W., 1991. The Lunar environment. In: G. Heiken, D. Vaniman and B.M. French, eds. *Lunar Sourcebook: A User's Guide to the Moon*. Cambridge: Cambridge University Press. pp.27–60.

Venugopal, I., Muthukkumaran, K., Annadurai, M., Prabu, T. and Anbazhagan, S., 2020. Study on geomechanical properties of lunar soil simulant (LSS-ISAC-1) for chandrayaan mission. *Advances in Space Research*, [online] 66(11), pp.2711–2721. Available at: <<https://doi.org/10.1016/j.asr.2020.08.021>>.

Warren, P., 1985. The Magma Ocean Concept and Lunar Evolution. *Annual Review of Earth and Planetary Sciences*, 13(1), pp.201–240.

White, L.F., Bailey, I., Foster, G.L., Allen, G., Kelley, S.P., Andrews, J.T., Hogan, K., Dowdeswell, J.A. and Storey, C.D., 2016. Tracking the provenance of Greenland-sourced, Holocene aged, individual sand-sized ice-rafted debris using the Pb-isotope compositions of feldspars and ⁴⁰Ar/³⁹Ar ages of hornblendes. *Earth and Planetary Science Letters*, [online] 433(November 2015), pp.192–203. Available at: <<http://dx.doi.org/10.1016/j.epsl.2015.10.054>>.

Wood, J.A., Dickey, J.S.J., Marvin, U.B. and Powell, B.N., 1970. Lunar anorthosites and a geophysical model of the moon. In: *Apollo 11 Lunar Science Conference*. Houston: Lunar and Planetary Institute. pp.965–988.

Wright, E., 2019. *Apollo Landing Sites with Moon Phases*. [online] Available at:






<<https://svs.gsfc.nasa.gov/4731>>.

Xu, Z., Guo, D. and Liu, J., 2021. Maria basalts chronology of the chang'E-5 sampling site. *Remote Sensing*, 13(8), pp.1–17.


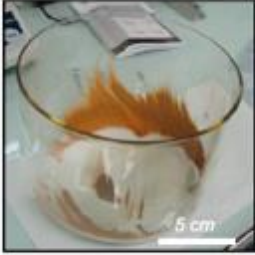
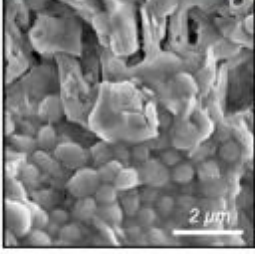
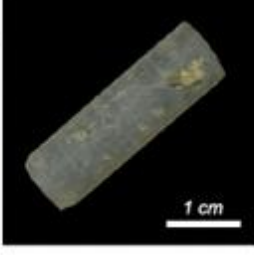
Zhang, X., Osinski, G.R., Newson, T., Ahmed, A., Touqan, M., Joshi, D. and Hill, H., 2019. A Comparative Study of Lunar Regolith Simulants in Relation to Terrestrial Tests for Lunar Exploration Missions. In: *50th Lunar and Planetary Science Conference 2019*. Houston: Lunar and Planetary Institute.

Zheng, Y., 2005. *Development of Lunar Soil Simulants and Characteristics of Microwave Radiation of Lunar Regolith*. Institute of Geochemistry, Chinese Academy of Sciences.

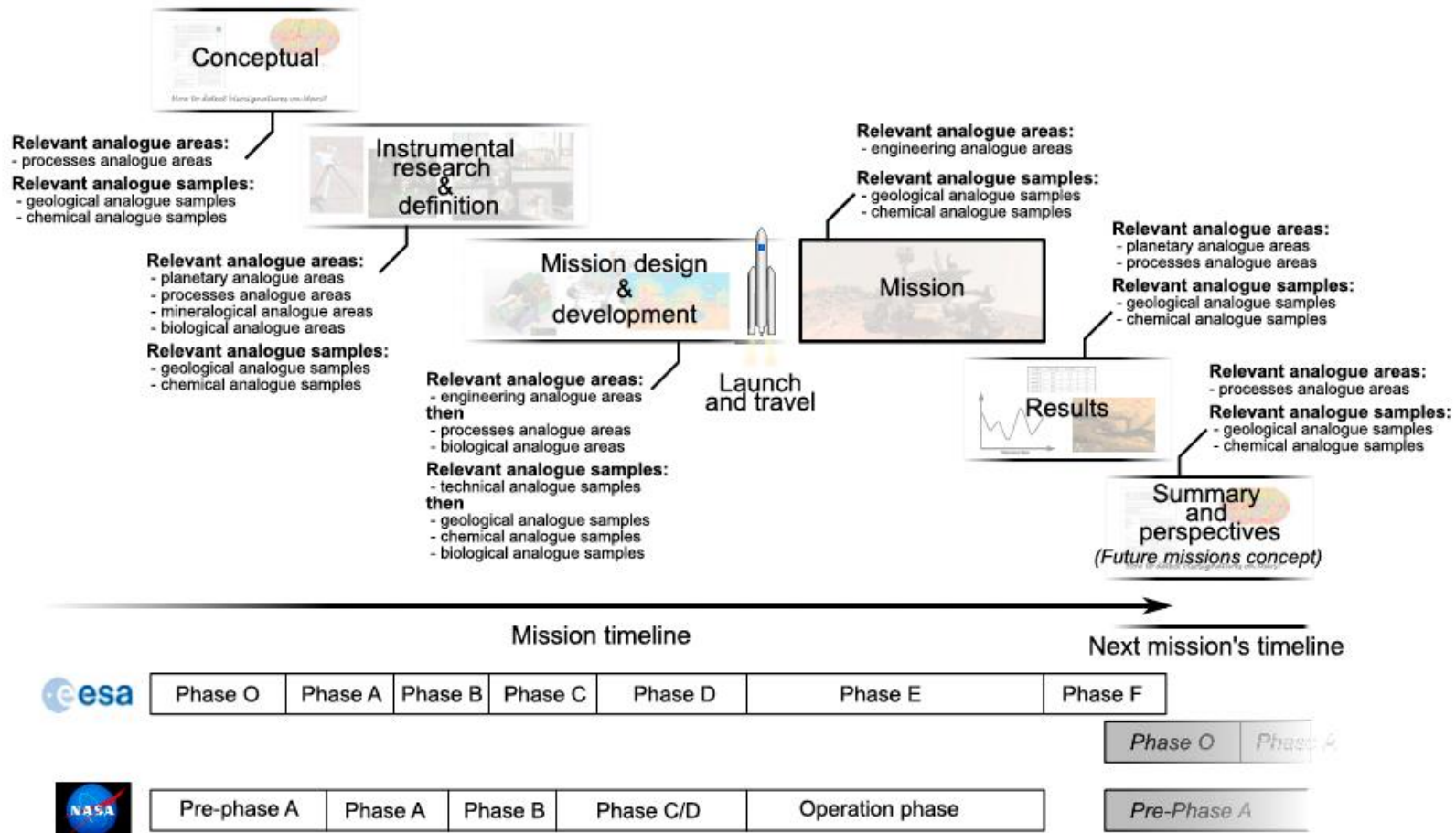
Appendices

Planetary		<p>Relevance Large scale geological structures, geomorphology, landscape</p> <p>Use Explain and/or illustrate observed or expected extraterrestrial geological structures, astronaut training (scientific)</p> <p>Analogy limitation Environmental conditions, lithology</p>
Process		<p>Relevance Mechanical and/or chemical alteration processes, transportation, hydrothermalism, impact, metamorphism, weathering</p> <p>Use Explain and/or illustrate observed or expected extraterrestrial geological processes</p> <p>Analogy limitation Origin of the processes, environmental conditions, petrography</p>
Petrology		<p>Relevance Mineral formation</p> <p>Use Collection of minerals</p> <p>Analogy limitation Formation processes, geological setting</p>
Astrobiology		<p>Relevance Extinct or extant life in analogue environmental conditions</p> <p>Use Study metabolism in analogue conditions, search for detectable biosignatures of present or past traces of life</p> <p>Analogy limitation Speculative analogy with extraterrestrial life</p>
Engineering		<p>Relevance Topography, mechanical and physical properties of the surface, environmental conditions, facilities</p> <p>Use Rover and instrumental testing, astronaut training (practical)</p> <p>Analogy limitation Nature of the obstacles, environmental conditions</p>

Appendix A-1. Examples of large-scaled analogue sites (Foucher et al., 2021).

Geological analogue		<p>Relevance Rocks, minerals</p> <p>Use Science and instrument testing</p> <p>Analogy limitation Elemental and mineralogical composition, material properties</p>
Chemical analogue		<p>Relevance Organic and inorganic molecules</p> <p>Use Science and instrument testing</p> <p>Analogy limitation Mixture composition</p>
Biological analogue		<p>Relevance Extant or extinct life from analogue areas, living organisms</p> <p>Use Study metabolism in analogue conditions, search for detectable biosignatures of present or past traces of life, test the limit of life</p> <p>Analogy limitation Speculative analogy with extraterrestrial life</p>
Technical analogue		<p>Relevance Mechanical and/or physical properties</p> <p>Use Instrument testing and training</p> <p>Analogy limitation Composition</p>

Appendix B-2. Examples of small-scaled analogue samples (Foucher et al., 2021).



Appendix C-3. Relevant functional analogues at each phase of a planetary exploration mission (Foucher et al., 2021).

Appendix D. List of properties in lunar simulants in the order of importance in research. Ranking arranged based on consensus count of the 2005 Lunar Regolith Simulant Materials Workshop (Sibille et al., 2006).

Order of importance	Property category	Property
1	Grain	Grain size
2	Grain	Grain size distribution
3	Physical	Particle density
4	Chemical	Glass content
5	Physical	Bulk density
6	Modal composition	As a function of grain size
7	Grain	Grain shape
8	Chemical	Bulk chemistry
9	Grain	Magnetic property
10	Geomechanical	Mechanical strength/ Compressibility
11	Composition	Total modal composition
12	Geomechanical	Mechanical strength – friction coefficient
13	Physical	Porosity
14	Chemical	Reactivity as volatile/soluble mineral
15	Implanted solar particles	

16	Grain	Grain shape distribution
17	Electrostatic charging	
18	Geomechanical	Shear strength
19	Geomechanical	Fatigue
20	Physical	Thermal properties
21	Physical	Surface area
22	Physical	Friability
23	Geomechanical	Strength/grain hardness
24	Geomechanical	Rheology
25	Geomechanical	Repose angle
26	Physical	Permeability
27	Geomechanical	Tensile
28	Geomechanical	Fracture
29	Chemical	Reactivity from surface damage
30	Texture	
31	Agglutinate	Single domain iron
32	Geomechanical	Impact resistance

Appendix E. List of capability levels in replicating lunar regolith properties into simulants (LEAG and CAPTEM, 2010).

1. Proven capability to reproduce
 - a. Agglutinates
 - b. Mineralogically-correct grains
 - c. Particle size distribution between the range of 5 μm and 5 mm
 - d. Synthesizing minerals, including high-An plagioclase, pyroxenes, glasses, breccias, commercial whitlockite, and ilmenite (with possible minor contamination)
 - e. Basaltic and anorthositic compositions
2. Potential to be reproduced but not proven
 - a. Small-size glass beads
 - b. Particle size distributions smaller than 5 μm or larger than 5 mm
 - c. Less than 0.1% Loss on Ignition (LOI) when quantity is more than a few kilograms
3. Cannot yet produce
 - a. Particle textures other than agglutinates
 - b. Vapour-deposited rims
 - c. Trace elements patterns
 - d. Minor and trace mineralogy
 - e. Shocked features in the particles
 - f. Orthopyroxene and clinopyroxene ratio
 - g. Specific mineralogy nuances (e.g. high-Fe feldspars)
4. Unknown capability to reproduce
 - a. Particle shape distributions
 - b. Relationships between particle sizes, shapes and compositions

Appendix F. Possible Sources of Errors and Contaminations

1. Processing impact rocks and Greenspar
 - a. Crusher and pan
 - b. Pulverizer container
 - c. Transferring of products

2. XRD
 - a. Mortar and pestle
 - b. Ethanol

3. Physical and geotechnical characterization
 - a. Sieves and sieve shaker
 - b. Proctor compaction test cylinder
 - c. Oedometer container

Appendix G: Consolidation Results

Vertical Stress (kPa)	LHS-1	UWO-1G	Breccia	Melt
5	0.767	0.84	1.117	0.891
10	0.756	0.818	1.064	0.874
20	0.738	0.802	1.015	0.851
40	0.713	0.786	0.969	0.822
80	0.687	0.767	0.924	0.788
160	0.658	0.747	0.88	0.751
320	0.627	0.723	0.835	0.711
640	0.591	0.695	0.786	0.667
320	0.601	0.704	0.797	0.677
160	0.609	0.713	0.805	0.688
80	0.62	0.72	0.817	0.694
40	0.626	0.724	0.822	0.699
20	0.63	0.727	0.826	0.703
10	0.633	0.73	0.83	0.706
Maximum void ratio difference (kPa)	0.165	0.123	0.278	0.207

Curriculum Vitae

Name: Xiaochen Zhang

Post-secondary Education and Degrees: University of Waterloo
Waterloo, Ontario, Canada
2008-2012 B.Sc.

International Space University
Illkirch-Graffenstaden, France
2016-2018 M.Sc.

University of Western Ontario
London, Ontario, Canada
2019-2021 M.Sc.

Honours and Awards: University of Waterloo Earth Sciences Entrance Scholarship
2008

International Space University Entrance Scholarship (Provided by the European Space Agency)
2016

Tohoku University Research-Oriented Incoming Student Scholarship
2017

MEXT Grant-in-Aid for Scientific Research on Innovative Areas
2017

International Space University Graduate Scholarship (Provided by the European Space Agency)
2018

Related Work Experience Teaching Associate
International Space University
2021

Teaching Assistant
The University of Western Ontario
2019-2020

Publications:

Evellin, P.; van Oorschot, J.; Harding, A.; Frayling, A.; **Zhang, X.**; Fernandes, M.; Ioda, S. (2017), *Reassessing the Moon Village Roadmap*, International Astronautical Congress, Adelaide, Australia.

Kokotailo, J.; Dao, L.; Scanlan, M.; Bidard, T.; Gevargiz, R.; Volohonsky, G.; Hussein, H.; Fernandes, M.; **Zhang, X.**; Li, B.; Cavallini, A.; Kawade, P.; Cabrera, N.; Ouyang, Y.; Zhai, M.; Xie, C.; Ozkan, F.; Ma, C.; Liu, S.; Harrison, S. (2017), *The Rise of Drones: Analysis of Current and Future Applications of Drones in Terrestrial Remote Sensing*, International Astronautical Congress, Adelaide, Australia.

Zhang, X.; Osinski, G.R.; Newson, T.; Touqan, M.; Joshi, D.; Hill, H. (2019), *A Comparative Study of Lunar Regolith Simulants in Relation to Terrestrial Tests for Lunar Exploration Missions*; Lunar and Planetary Science Conference (Poster), The Woodlands, Texas, USA.

Zhang, X.; Osinski, G. R., Newson, T.; Touqan, M.; Joshi, D.; Hill, H. (2019), *Comparison of Selected Lunar Regolith Simulants and Implications on Their Potentials for ISRU-Related Applications*; Lunar ISRU 2019 (Poster), Columbia, Maryland, USA.

Zhang, X.; Stupar, D. (2019), *The Primary Locations and Settlement Strategies of Interest for Future Lunar Bases*; International Astronautical Congress (Abstract), Washington D.C., USA.

Newson, T; Ahmed, A; Joshi, D; **Zhang, X**; Osinski, G.R. (2020), *Assessment of the Geomechanical Properties of Lunar Simulant Soils*; ASCE Earth & Space, Seattle, Washington, USA. (Conference deferred to 2021 due to COVID-19)

Newson, T; Ahmed, A; Joshi, D; Zhang, X; Osinski, G. R. (2021), *Assessment of the Geomechanical Properties of Lunar Simulant Soils*; Canadian Lunar Workshop (Virtual event).